Hearing Research 424 (2022) 108568

Contents lists available at ScienceDirect

Hearing Research

journal homepage: www.elsevier.com/locate/heares

Audiologic characterization using clinical physiological measures: Normative data from macaque monkeys

Amy N. Stahl[1,2], Jane A. Mondul[1,2], Katy A. Alek[2], Troy A. Hackett[2], Ramnarayan Ramachandran[2,*]

[1] Vanderbilt Neuroscience Graduate Program, Vanderbilt University, Nashville, TN 37212
[2] Vanderbilt Department of Hearing and Speech Sciences, Vanderbilt University Medical Center, Nashville, TN 37212

ARTICLE INFO

Article history:
Received 4 April 2022
Revised 28 June 2022
Accepted 8 July 2022
Available online 12 July 2022

Keywords:
Physiology
electrophysiology
auditory brainstem response
distortion product otoacoustic emissions
nonhuman primates
peripheral auditory function

ABSTRACT

Clinical auditory physiological measures (e.g., auditory brainstem responses, ABRs, and distortion product otoacoustic emissions, DPOAEs) provide diagnostic specificity for differentially diagnosing overt hearing impairments, but they remain limited in their ability to detect specific sites of lesion and subtle levels of cochlear damage. Studies in animal models may hold the key to improve differential diagnosis due to the ability to induce tightly controlled and histologically verifiable subclinical cochlear pathologies. Here, we present a normative set of traditional and clinically novel physiological measures using ABRs and DPOAEs measured in a large cohort of male macaque monkeys. Given the high similarities between macaque and human auditory anatomy, physiology, and susceptibility to hearing damage, this normative data set will serve as a crucial baseline to investigate novel physiological measures to improve diagnostics. DPOAE amplitudes were robust at $f_2 = 1.22$, $L_1/L_2 = 65/55$, increased with frequency up to 10 kHz, and exhibited high test re-test reliability. DPOAE thresholds were lowest from 2-10 kHz and highest < 2 kHz. ABRs with a standard clinical electrode montage (vertex-to-mastoid, VM) produced Waves I-IV with a less frequently observed Wave-I, and lower thresholds. ABRs with a vertex-to-tympanic membrane (VT) electrode montage produced a more robust Wave-I, but absent Waves II-IV and higher thresholds. Further study with the VM montage revealed amplitudes that increased with stimulus level and were largest in response to click stimuli, with Wave-II showing the largest ABR amplitude, followed by -IV and -I, with high inter- and intra-subject variability. ABR wave latencies decreased with stimulus level and frequency. When stimulus presentation rate increased or stimuli were presented in close temporal proximity, ABR amplitude decreased, and latency increased. These findings expand upon existing literature of normative clinical physiological data in nonhuman primates and lay the groundwork for future studies investigating the effects of noise-induced pathologies in macaques.

1. Introduction

and Audiologic assessments aim to identify site and degree of lesion in the auditory pathway and obtain information regarding the perceptual and functional consequences of the lesion (Hall, 2017; Stach and Ramachandran, 2021). By design, the standard clinical test battery is focused on identifying a decreased ability to detect low level sounds as decreased hearing sensitivity is characteristic of most clinically identifiable forms of peripheral auditory pathology including sensorineural, conductive, and mixed hearing losses. The degree and type of hearing loss can be assessed behaviorally, or estimated physiologically using the auditory brainstem response (ABR) (Stapells and Oates, 1997). The graphical depiction of these results, known as an audiogram, illustrates hearing sensitivity as a function of tone frequency and is used for therapeutic purposes, including the programming of hearing aids to restore the loss of sensitivity. In addition to the audiogram, the differential diagnosis between types of peripheral hearing loss and the identification of risk factors for retro-cochlear pathology (e.g., auditory neuropathy, acoustic neuroma, vestibular schwannoma) can be assessed through tympanometry (differential diagnosis of middle ear involvement: Lidén et al., 1970), screening or threshold measurement of the ipsilateral and/or contralateral middle ear muscle reflex (MEMR) (differential diagnosis of cochlear vs. retro-

* Send correspondence to: Ramnarayan Ramachandran, Ph.D., Department of Hearing and Speech Sciences, Vanderbilt University School of Medicine, 111 21st Ave. South, Wilson Hall 065, Nashville, TN 37212, (615) 322-4991 (phone), (615) 343-0884 (fax)

E-mail addresses: amy.n.stahl@vanderbilt.edu (A.N. Stahl), jane.a.burton@vanderbilt.edu (J.A. Mondul), Catherine.a.alek@vumc.org (K.A. Alek), troy.a.hackett@vanderbilt.edu (T.A. Hackett), ramnarayan.ramachandran@vumc.org (R. Ramachandran).

https://doi.org/10.1016/j.heares.2022.108568
0378-5955/

cochlear: Anderson et al., 1969; differential diagnosis of conductive vs. sensorineural: Feldman, 1977; Jerger et al., 1974), screening of distortion product otoacoustic emissions (DPOAEs) (Starr et al., 1996), and/or measurement of supra-threshold speech perception (Hurley and Sells, 2003; Thornton and Raffin, 1978).

Although this diagnostic toolbox clearly allows for differentiation between relatively major sites of auditory lesion in the peripheral pathway (e.g., outer and/or middle ear, inner ear and/or more central, or both), there has emerged a need for diagnostic tools that can identify and differentiate between subtle physiological differences within the extensive umbrella of cochlear pathology. This is highlighted by the large individual differences seen in supra-threshold speech perception performance (in both quiet and noise) in patients with similar degrees of sensorineural hearing loss (Wilson et al., 2010), and is further highlighted by the 5-15% of patients seeking audiological care for perceived supra-threshold speech perception difficultly (primarily in noise) who have clinically normal hearing (Hind et al., 2011; Spankovich et al., 2017). Both examples, although on two different ends of the same spectrum, suggest the presence of unidentified physiological changes causing perceptual deficits in a significant proportion of the patient population. This high prevalence of such unexplained auditory deficits (Smith et al., 2019) has led to the term and label of hidden hearing loss (HHL). The underlying causes of such HHL have been suspected to include, but may not be limited to, subclinical outer hair cell (OHC) loss or damage (Di Mauro et al., 2019); subclinical inner hair cell (IHC) loss or damage (Lobarinas et al., 2016); loss or damage to synaptic connections between IHCs and auditory nerve fibers (ANFs) (also referred to as cochlear synaptopathy; SYN) (Kujawa and Liberman, 2009); and ANF demyelination (Kohrman et al., 2020).

To identify an objective diagnostic tool sensitive to subtle amounts of cochlear damage for the purpose of translation to human clinical populations, there must be a correlation between the confirmed pathology of interest and a change in a non-invasive measure of physiological function. Animal models offer the unique ability to investigate such relationships using confirmed and controlled subclinical cochlear pathology. Given the candidate cochlear sites proposed to underlie hidden hearing loss (i.e., OHCs, IHCs, IHC ribbon synapses, and ANFs), measures of physiological function that are known to identify clinically significant amounts of damage to OHCs (i.e., DPOAEs, ABRs) (Kemp, 2002) and IHCs/ANFs (i.e., ABRs) (Buchwald and Huang, 1975) are being investigated to determine if they may also be useful in identifying more subtle amounts of damage. In addition to standard clinical DPOAE and ABR metrics, clinically novel metrics and stimulus paradigms that were designed to tax auditory peripheral processing power are also being investigated for sensitivity to subtle peripheral damage that may be missed with traditional measures. Before the diagnostic sensitivity of these measures can be addressed in studies involving perturbations to the auditory system, normative datasets must be established. To increase the likelihood of successful translation of these candidate diagnostic tools to human populations, normative characterization in a range of species may be advantageous. While several studies have investigated novel DPOAE and ABR metrics in rodents (e.g., ABR presentation rate: Newton et al., 1992; DPOAE thresholds and input-output functions: Parham, 1997), nonhuman primates (NHPs) are an invaluable model of human hearing and inner ear disorders because of their comparable auditory anatomy, physiology, genetic heterogeneity, perceptual capabilities, and susceptibility to hearing damage (Burton et al., 2019; Gibbs et al., 2007; Valero et al., 2017). Additionally, comparison of normative data collected with different recording techniques within a single species may help identify the most sensitive diagnostic approaches.

The present study seeks to establish normative physiological data from normal hearing macaque monkeys using traditional and novel audiologic characterization of ABR and DPOAE responses. Our study builds upon the body of normative ABR and DPOAE data in macaques by creating a single reference with a comprehensive test battery in a young adult cohort. Previous macaque studies established normative DPOAE amplitudes (e.g., Park et al., 1995; Torre and Fowler, 2000), ABR amplitudes and latencies to single clicks (e.g., Allen and Starr, 1978; Doyle et al., 1983; Kraus et al., 1985), and ABR amplitudes and latencies to tonebursts (Lasky et al., 1999). Single studies also assessed normative tympanometry (Torre et al., 2000), DPOAE thresholds (Lasky et al., 1999), and the effect of click rate on ABRs (Allen and Starr, 1978). However, the existing macaque literature is limited by smaller sample sizes and transformed data that make it difficult to extract normative values (e.g., Allen and Starr, 1978; Ng et al., 2015; Park et al., 1995) and/or the use of slightly older adult macaques (Lasky et al., 1999). Here, we extend this prior work by reporting the following physiologic measures, including: tympanometry, DPOAE amplitudes and thresholds; ABR amplitudes, latencies, and thresholds in response clicks and tone bursts; ABR amplitude ratios in response to clicks and tone bursts; ABRs to clicks with varying presentation rates; and ABRs to click pairs with varying inter-click intervals. Additionally, this is the first macaque study to compare and contrast ABRs derived from both mastoid and tympanic membrane electrode placements. This is advantageous because both electrode placement locations are commonly used in clinical settings depending on structure of interest and the diagnostic goal of the recording (e.g., use of ECochG is common for enhancement of the cochlear microphonic, summating potential, and Wave-I, diagnosis of Meniere's Disease, auditory neuropathy spectrum disorder, and for intraoperative monitoring) (Ferraro and City, 2000; Ferraro and Tibbils, 1999; Krieg et al., 2014). Thus, these data may help guide electrode choice in future macaque studies that have clinical, translational, and diagnostic focuses.

2. Material and methods

2.1. Subjects

Thirty-six male macaque monkeys (*Macaca mulatta,* n=34*, and Macaca radiata,* n=2) were included in this study with some measures collected in only a subset of subjects. All monkeys were between the ages of 6-10 years. Macaque monkeys reach sexual maturity by 5 years of age and have a maximum recorded lifespan of 40 years in the wild and approximately 25-30 years in captivity (Chiou et al., 2020; Roth et al., 2004).The macaques used in this study were approximately equivalent to 18-30 years of age for humans (see Davis and Leathers, 1985). Age-related changes to the auditory system were not a concern (Ng et al., 2015). Monkeys were obtained from various sources, including the California National Primate Research Center at the University of California Davis, the Oregon National Primate Research Center, the Children's Hospital of Pennsylvania, and commercial vendors such as Covance. They were housed at Vanderbilt University on a 12-hour light/dark cycle and provided with access to a carefully controlled diet *ad libitum*, except for 12-18 hours prior to sedated procedures for physiological testing. For some monkeys involved in behavioral tasks, access to water was restricted. These monkeys were subject to surgical procedures to implant instrumentation that would fix their heads in standard orientation during behavioral tasks, to facilitate similar relationship between sound source and ears across sessions. Neither water restriction, nor the implantation of cranial instrumentation influenced any of the measures discussed below ($p > 0.05$, Wilcoxon Rank Sum). Thus, the groups with and without water restriction and cranial instrumentation were combined. All housing and procedural protocols were approved by the Institutional Animal Care and Use Committee (IACUC) at the Vanderbilt University

Medical Center and were in strict compliance with the guidelines established by the National Institutes of Health (NIH).

Subjects were excluded from the study if they possessed abnormal outer or middle ear function and/or abnormal outer hair cell function as measured during otoscopy, tympanometry, and DPOAE testing. The specific criteria and the number of subjects excluded by these measures is detailed in later sections.

2.2. Sedation

Subjects were sedated for the entirety of physiological testing. Immediately prior to sedation, macaques were treated with atropine (0.04 mg/kg) to minimize mucous secretions. Then, subjects were initially anesthetized with a cocktail of ketamine (10 mg/kg i.m.) and midazolam (0.05 mg/kg i.m.), moved from their home cage to a surgical suite, positioned prone with their head slightly elevated and the neck extended, and intubated. They were then moved to a sound treated room where they were switched to a breathing circuit and maintained with 1-2% isoflurane for the remainder of testing.

2.3. Otoscopy

Visual inspection of the external auditory canal and tympanic membrane was performed using an otoscope (Welch Allyn, 25020 3.5V Halogen Otoscope Head) to assess for contraindications to completing physiological testing. These contraindications included excessive cerumen and/or debris, active otorrhea, and tympanic membrane perforation/bulging/retraction.

2.4. Tympanometry

Following otoscopic inspection, standard clinical tympanometry was completed using a calibrated Amplivox Otowave tympanometer. A 226-Hz probe tone was generated in the ear canal while the ear canal pressure was systematically swept from +200 to -300/400 daPa. Changes in probe level during the pressure sweep resulted in estimates of tympanic membrane compliance (mL), middle ear pressure (daPa), and ear canal volume (cc). Tympanometry was evaluated to establish normative data in macaques. Subjects with very large ear canal volumes (>1.0 cc), very small ear canal volumes (<0.2 cc), or middle ear pressure values that were < -150 daPa were excluded from the study due to likely tympanic membrane perforation, cerumen impaction, or middle ear dysfunction.

2.5. Distortion product otoacoustic emissions (DPOAEs)

A Scout Biologic OAE System (Natus) was used to measure DPOAEs at eight frequencies per octave from f_2 = 0.5-10 kHz. In an initial subset of subjects, frequency ratios and level ratios of the primary tones were varied (L_1/L_2 ratios of 70/70, 65/55 dB SPL; f_2/f_1 ratios of 1.15, 1.20, 1.22, 1.25) to identify optimal stimulus parameters to achieve the strongest emissions in this species. Following parameter optimization, a DP-gram was measured in all subjects using an L_1/L_2 ratio of 65/55 and an f_2/f_1 ratio of 1.22. Subjects with *absent* (defined in the next section) DP-grams at L_1/L_2 = 65/55 dB SPL were excluded from subsequent testing due to outer hair cell dysfunction. Subjects with *present* (defined in next section) DP-grams at L_1/L_2 = 65/55 dB SPL were included in subsequent testing in which DPOAEs were collected for increasing stimulus levels (5-dB SPL steps) from L_1/L_2 = 30/20 dB SPL to L_1/L_2 = 80/70 dB SPL while the difference between L_1 and L_2 remained stable at 10 dB SPL. The DPOAEs collected at increasing stimulus levels were used to derive threshold-versus-frequency and input-output functions.

2.5.1. DPOAE data analysis

In accordance with the Vanderbilt audiology clinic criteria, distortion products at $2f_1$-f_2 were considered *present* if the DPOAE amplitude was at least 0 dB SPL and at least 6 dB above the noise floor. *Threshold* was defined as the lowest f_2 level required to produce a distortion product that was considered present. Although stimulus levels did not extend beyond L_1/L_2 = 80/70 dB SPL due to the limits of the Scout Biologic OAE System, this was typically not a concern for deriving threshold. Furthermore, high sound level evoked DPOAEs are diagnostically unreliable for stimulus levels that increase beyond L_1/L_2 = 80/70 dB SPL as OHC somatic motility is no longer necessary for DPOAE production (Liberman et al., 2004). Of note, through the course of establishing and optimizing DPOAE data, slightly differently acquisition protocols were used across subjects (e.g. number of points per octave, specific f_2 frequencies used). For the sake of maximum transparency, we reported the number of ears that were tested at each frequency, which led to variability in sample size across data points as indicated by the ranges in the DPOAE figure legends (e.g., n = 46-61 ears in Figure 3A).

2.6. Auditory brainstem responses (ABRs)

ABRs were recorded in response to broadband clicks (0.001-97 kHz; 100μs duration; 27.7/s) and frequency-specific tone bursts (0.5 – 32 kHz; 27.7/s) that span much of the audible range of macaques (Pfingst et al., 1978). Tone burst stimuli had frequency dependent rise/fall times and plateau durations that matched those used by the Vanderbilt audiology clinic (rise/fall times: 1ms (2-32 kHz), 2ms (1 kHz), or 4ms (0.5 kHz); plateau durations: 0.5 ms (2-32 kHz), 1 ms (1 kHz) or 2 ms (0.5 kHz)).

Two electrode montages were used to determine their respective influence on waveform morphology, amplitude, and threshold. In the vertex-to-tympanic membrane (VT) montage, the active electrode was placed directly on the tympanic membrane using a tympanic ball electrode (Sanibel) using electrode gel (Nuprep, Weaver and Company) to reduce impedance. In the vertex-to-mastoid (VM) montage, the active electrode was placed on the mastoid using a subdermal needle electrode (Rhythmlink). For both electrode montages, a reference subdermal needle electrode was placed at the vertex, and a ground subdermal needle electrode was placed at the shoulder. All electrode impedances were $\leq$ 3 kΩ.

After obtaining waveform morphologies, amplitudes, and thresholds that were more optimal with the VM montage compared to the VT montage (see Results), further normative ABR characterization was completed only using the VM montage in response to clicks of varying presentation rates (27.7/s, 57.7/s, 100/s, 125/s, 166.6/s, 200/s; 70-90 dB SPL) and click pairs of varying interclick intervals (ICIs) (1, 2, 4, 8, and 10ms; 70-90 dB SPL).

2.6.1. ABR stimulus calibration, generation, and delivery

The tympanic ball electrode that was used to record with the VT electrode montage partially occluded the subjects' ear canals. Thus, a sound-field speaker (NuScale 216, Rhyme Acoustics) was used to present stimuli during VT electrode montage recordings. In contrast, the subdermal needle electrode placed on the mastoid that was used to record with the VM electrode montage allowed unrestricted access to the subjects' ear canals. This permitted the use of a calibrated closed-field speaker (MF1, Tucker-Davis Technologies) coupled to a disposable foam eartip (ER3-14 B 10mm, Etymotic Research) to monaurally present stimuli during VM electrode montage recordings.

Free-field stimuli were amplified using an SLA2 amplifier (ART Pro Audio, Niagara Falls, NY) and calibrated to produce appropriate sound levels (+/- 3 dB) using a ¼ inch free-field microphone (378C01, PCB Piezotronics) positioned at the location where the

subjects' head would be during experiments. Closed-field stimuli were calibrated (+/- 3 dB) using a 0.5cc coupler and verified in the ear canal using a probe microphone system (Fonix 8000, Frye). Stimuli for both VT and VM montages were created in SigGenRZ software (Tucker-Davis Technologies), generated by an RZ6 Multi-I/O Processor (Tucker-Davis Technologies) using BioSigRZ software (Tucker-Davis Technologies), and presented using an alternating stimulus polarity for two separate runs of 1024 presentations.

2.6.2. ABR signal recording

During online recording, either the combination of a RA4LI low impedance head stage with a RA4PA preamplifier (VT montage), or a Medusa 4Z preamplifier (Tucker-Davis Technologies) (VM montage) amplified the incoming signal (10,000x), which was digitally filtered from 0.3-3 kHz. Signals with amplitudes greater than 1 mV were rejected using the Artifact Rejection feature in BioSigRZ, and not included in the 1024 averages.

2.6.3. ABR data analysis

During offline analyses, two traces of 1024 artifact-free waveforms were averaged together, inverted (for VM montage only; completed to display ABR waveforms in the traditional upright/positive deflection orientation for this electrode montage), and low-pass filtered at 1.5 kHz to produce a final ABR trace. Low-pass filtering was completed to reduce noise by isolating the ABR signal spectrum, which is limited to below approximately 1.5 kHz (Boston, 1981). Then, using this final ABR trace, the amplitude and latency of each waveform component and the threshold for each ABR frequency were determined.

The *amplitude* of a waveform component was defined as the peak-to-trough amplitude, or the maximum positive to maximum negative deflection (in nV) of the respective wave. Peaks and troughs were identified manually by experienced audiologists and research personnel. The *latency* of a waveform component was defined as the time (in ms) between stimulus onset and the maximum positive deflection (i.e., peak) of the wave of interest. Of note, some subjects only had some, or did not have any, waveforms components that were identifiable above the noise floor at lower stimulus levels (e.g., 30 dB SPL) or lower stimulus frequencies (e.g., 0.5 or 1 kHz), which meant that the amplitude and latency of these waveform components could not be analyzed. This resulted in the variability in sample size reported in the ABR figure legends (e.g., the *n* ranges from 5-28 ears for Wave-I as the stimulus increased from 30 to 90 dB SPL in Figure 6A).

To determine *threshold*, a modified Hughson Westlake procedure (Carhart and Jerger, 1959) was used: stimuli were presented at a starting level of 90-dB SPL, decreased in 10- to 20-dB increments until the evoked response was no longer visually identifiable, and increased in 5-dB increments until the evoked response was visible. *Threshold* was then defined as the lowest sound level (to the nearest 5-dB SPL) at which any repeatable wave (i.e., Wave-I, -II, or -IV) could be identified and was significantly above the noise floor.

Also of note, for the waveform traces that were recorded in response click pairs at *short* inter-click intervals (i.e., click pairs that were separated by 4, 2, and 1ms), the evoked response to Click 1 overlapped the evoked response to Click 2. Thus, the evoked response to Click 1 was subtracted from the waveform trace to reveal and allow analysis of the evoked response to Click 2. This was completed by subtracting the single click (27.7/s) waveform trace from the click pair waveform trace (as described in further detail in Lee et al., 2020) at 4, 2, and 1 ms.

2.7. Statistical analyses

Spearman rank correlation coefficients were used as a descriptive statistic for within and across session test-retest reliability of ABR wave amplitudes and latencies. The Spearman rank correlation is a non-parametric alternative to the Pearson correlation that is used to measure the degree of association between two variables made on the same subjects (Zar, 2005). Unlike the Pearson correlation coefficient, the Spearman rank correlation does not carry any assumptions about the distribution of the data. The Spearman rank correlation coefficient is the Pearson correlation coefficient between the rank variables.

Intraclass correlation coefficients (ICCs) (more specifically, ICC1s as defined by Shrout and Fleiss, 1979) were used to formally quantify the reliability of ABR wave amplitudes and latencies within and across test sessions. Unlike most other correlation measures, the ICC operates on data structured as groups, rather than data structured as paired observations. The ICC is commonly used in the assessment of the reproducibility of quantitative measurements of the same quantity. ICC1 is sensitive to differences in means between the observations and is a measure of absolute agreement. All statistical analyses were performed in Matlab (version R2017b) (Matlab, 2010).

3. Results

3.1. Outer and middle ear examination

Otoscopic examination revealed small, narrow ear canals that were best visualized with pediatric otoscope specula (2.5mm at their narrowest diameter). Middle ear status was evaluated using standard clinical tympanometric measures, including ear canal volume, tympanic membrane compliance, and middle ear pressure (n = 32 ears, 16 macaques). Ear canal volumes were found to be between 0.2 to 0.9 cc (M = 0.44, SD = 0.13) and tympanic membrane compliance values were found to be between 0.2 and 1.2 mmho (M = 0.57, SD = 0.22), consistent with previous data from macaques (Torre et al., 2000). Tympanometric peak pressure values were found to be between -94 and 72 daPa (M = -9.28, SD = 28.59). The 5th, 10th, 50th, 90th, and 95th percentiles for each tympanometric measure can be found in Table 1. Histograms for each measure are shown in Figure 1. Ear canal volume (Figure 1A) and compliance (Figure 1C) histograms revealed a similar range of data spread, however a tighter clustering around the mean value was found for ear canal volume compared to compliance. The histogram for middle ear pressure (Figure 1B) revealed a larger data spread, however a similar tight clustering around the mean value was found for pressure as seen with ear canal volume. Subjects with pinna abnormalities (n = 1), tympanic membrane perfora-

Table 1
5th, 10th, 50th, 90th, and 95th Percentiles of tympanometric measures

	5th Percentile	10th Percentile	50th Percentile	90th Percentile	95th Percentile
ECV (cc)	0.3	0.3	0.4	0.5	0.77
Compliance (mmho)	0.3	0.3	0.5	0.9	0.9
Pressure (daPa)	-50.0	-40.3	-9.0	13.0	54.4

Note. cc = cubic centimeters, mmho = millimho, daPa = decapascals, SD = standard deviation.

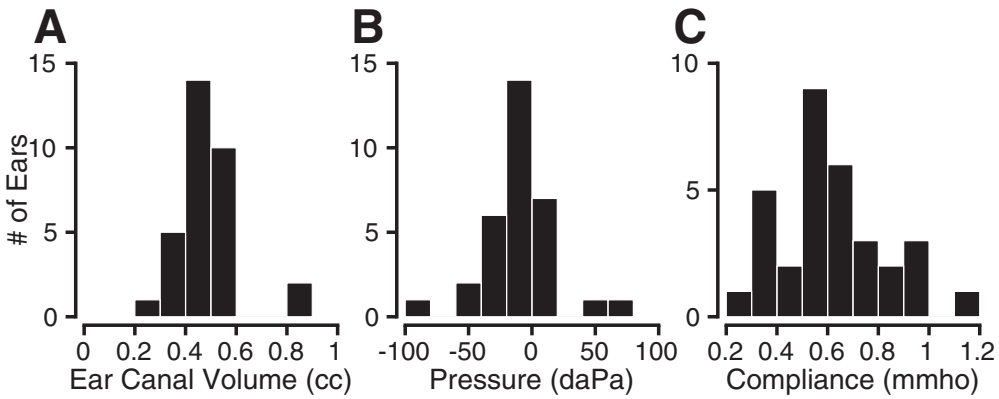

Figure 1. Histograms showing the number of ears (n = 32 ears, n = 16 macaques) as a function of 3 tympanometric measures: ear canal volume (A), pressure (B) and compliance (C). cc = cubic centimeters, mmho = millimho, daPa = decapascals.

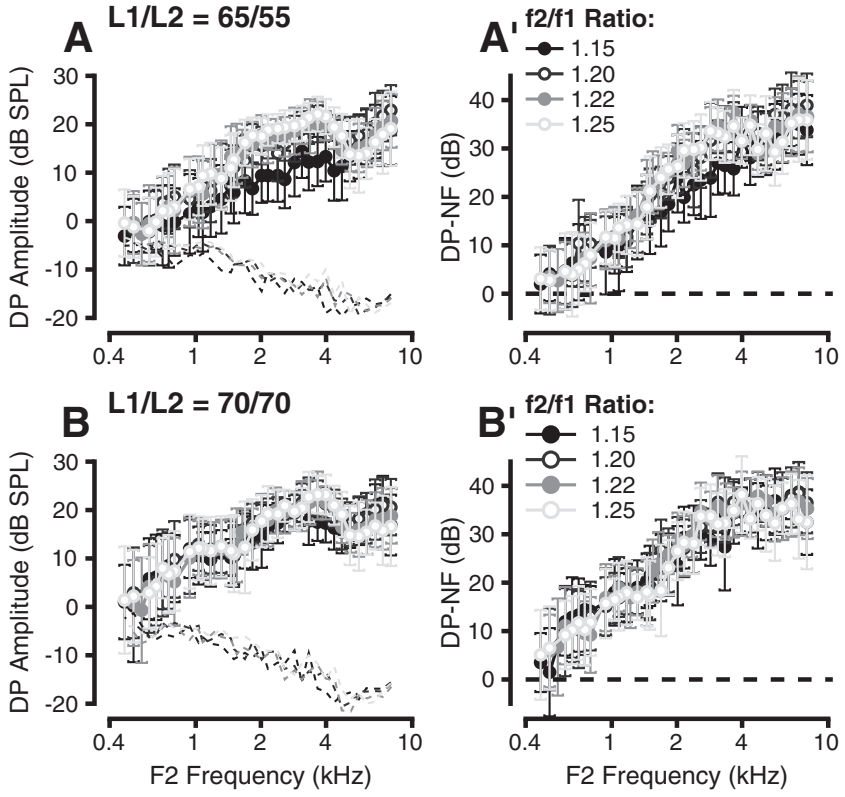

Figure 2. Optimization of stimulus frequency and level ratios (n = 20-24 ears). A, B. Average DP amplitude (dB SPL) (+/- 1 standard deviation, SD) as a function of f_2 frequency (kHz) in response to a stimulus presentation level of L_1/L_2 = 65/55 (A) and L_1/L_2 = 70/70 (B). A', B'. Average signal-to-noise ratio (SNR; DP amplitude - noise floor amplitude) (dB) (+/-1 SD) as a function of f_2 frequency (kHz) in response to a stimulus presentation level of L_1/L_2 = 65/55 (A') and L_1/L_2 = 70/70 (B').

tions (n = 2), or middle ear dysfunction (n = 5) (for details see Burton, 2022) were excluded from subsequent testing.

3.2. Distortion product otoacoustic emissions (DPOAEs)

3.2.1. Parameter optimization

Prior to establishing a normative DPOAE dataset, DPOAEs were measured on a subset of subjects (n = 20-24 ears) using a variety of frequency and level ratios of the primary tones to identify optimal stimulus parameters that evoked the strongest emissions. In this and other sections of the Results, we sometimes report a range of n-values, indicating the number of ears represented in each data point. These ranges resulted from slight variations in testing protocol across subjects. On average, all frequency (f_2/f_1 = 1.15, 1.20, 1.22, 1.25) and level ratio (L_1/L_2 = 70/70, 65/55) combinations tested resulted in strong DPOAEs for f_2 frequencies higher than 650 Hz, with DPOAE amplitudes well above the noise floor (Figure 2). Average DP amplitudes ranged from approximately 0 dB SPL in the low frequencies to 15-20 dB SPL in the high frequencies (Figure 2A, B). An L_1/L_2 ratio of 70/70 resulted in greater DPOAE amplitudes than the 65/55 level ratio for some frequency ratios, likely due to the higher stimulus levels (e.g., amplitudes at an f_2/f_1 ratio of 1.15 were 1.1-10.5 dB SPL greater across all frequencies for an L_1/L_2 ratio of 70/70 compared to 65/55; compare black filled circles in Figure 2A and 2B). However, since most frequency and level ratio conditions seemed similarly favorable, an f_2/f_1 ratio of 1.22 and an L_1/L_2 ratio of 65/55 were selected for further study to match human audiologic testing and allow for direct comparison with other animal species (Lasky et al., 1995a; Petersen et al., 2018).

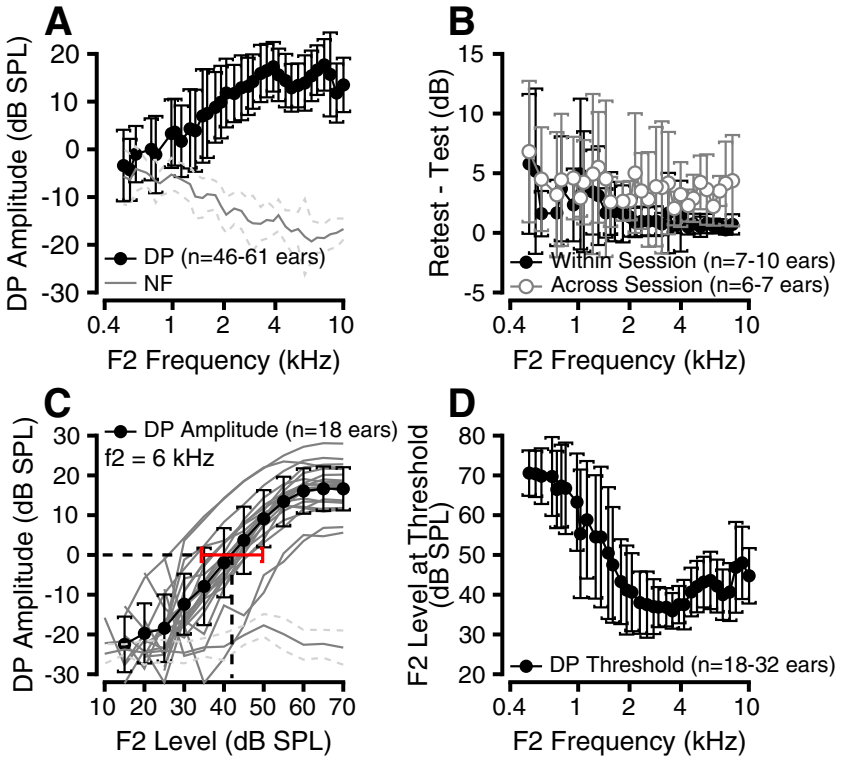

Figure 3. DPOAE amplitudes and thresholds using optimized stimulus parameters (f_2/f_1 = 1.22; L_1/L_2 = 65/55). A. Average DP amplitude (dB SPL) (+/- 1 SD) as a function of f_2 frequency (n = 46-61 ears). B. Average test-retest values (absolute value of DP_{retest} – DP_{test}) (+/- 1 SD) as a function of f_2 frequency. Filled black circles represent within session test-retest values (n = 7-10 ears). Unfilled gray circles represent across session test-retest values (n = 6-7 ears). C. Average DP amplitude (dB SPL) (+/- 1 SD) as a function of f_2 level (f_2 = 6kHz, L_1-L_2 = 10 dB; n = 18 ears). Dark gray lines represent individual ears. Light gray solid line surrounded by light gray dashed lines represent the average noise floor +/- 1 SD. The filled red circle represents average DPOAE threshold at f_2 = 6kHz; the red line represents +/- 1 SD of the threshold levels. D. Average f_2 level at DP threshold (dB SPL) (+/- 1 SD) as a function of f_2 frequency (n = 18-32 ears). (For interpretation of the references to color in this figure legend, the reader is referred to the web version of this article.)

3.2.2. Normative DPOAE amplitudes and thresholds

DPOAE amplitudes are shown as a function of f_2 frequency in Figure 3A (n = 46-61 ears per frequency). Emission amplitudes were at least 6 dB above the noise floor for frequencies greater than 650 Hz in most subjects (compare filled black circles with light gray lines). On average, emission amplitudes increased from 0.5-4kHz and plateaued at an average level of 10-15 dB SPL from 4-10kHz. Only one ear of one subject had grossly abnormal DPOAE amplitudes; this ear was excluded from all DPOAE and ABR results.

DPOAE test-retest reliability was assessed both within- and across-session for a subset of ears. Within-session measurements were made during the same procedure, and the DPOAE probe was removed from the ear and replaced back in the ear between Test 1 and Test 2. Across-session measurements were completed during separate procedures that took place approximately 1-1.5 years apart. Average test-retest values (absolute value of DP_{retest} – DP_{test}) are plotted as a function of f_2 frequency in Figure 3B. Within-session test-retest differences (filled black circles) ranged from 0.25-5.78 dB (n = 7-10 ears). Across-session test-retest differences (unfilled gray circles) ranged from 2.04-6.81 dB (n = 6-7 ears). Greater test-retest differences were observed for across-session tests and below 1kHz.

An additional DPOAE metric that is commonly used in animal research is the DPOAE threshold (e.g., Lasky et al., 1999; Shaffer and Long, 2004). For each f_2 frequency, DPOAEs were measured across a range of stimulus levels to derive input-output functions relating DP amplitude and f_2 level. Figure 3C shows input-output functions for 18 macaque ears (individual traces in gray; mean and standard deviation in black) in response to an f_2 of 6kHz ranging from 15- to 70-dB SPL. In accordance with standard clinical definitions of present otoacoustic emissions (Abdala and Visser-Dumont, 2001), threshold was defined as the lowest f_2 level that produced an emission that was ≥ 0 dB SPL in level and ≥ 6 dB above the noise floor. The mean DPOAE threshold at 6kHz is indicated by the dashed lines in Figure 3C (red bar represents +/- 1 standard deviation from the mean threshold) and is replotted with other DPOAE thresholds as a function of f_2 frequency in Figure 3D. Mean DPOAE thresholds were lowest (approximately 35-40 dB SPL) for f_2 frequencies between 2-10 kHz, similar to the range of frequencies eliciting the greatest suprathreshold DP amplitudes.

3.3. Auditory brainstem responses (ABRs)

3.3.1. Electrode montage optimization

Prior to establishing a normative ABR dataset, active electrode placement was varied between the ipsilateral mastoid (vertex-to-mastoid montage, VM) and the ipsilateral tympanic membrane (vertex-to-tympanic membrane montage, VT) to identify the effect(s) of electrode montage on waveform morphology, peak-to-trough amplitudes, and threshold. The VT electrode montage revealed two waveform components: a summating potential (SP) and an action potential (AP; synonymous with Wave-I), that decreased in amplitude as stimulus level decreased (Figure 4A). Despite the notable absence of Waves II-IV with the VT electrode montage, the VT electrode montage produced considerably larger Wave-I amplitudes compared to the VM electrode montage (see differences in the vertical scale bar between Figure 4A left column and Figure 4A right column), consistent with the VT electrode's closer physical proximity to the Wave-I generator site (Ferraro et al., 1986). In contrast, the VM electrode montage revealed four waveform compo-

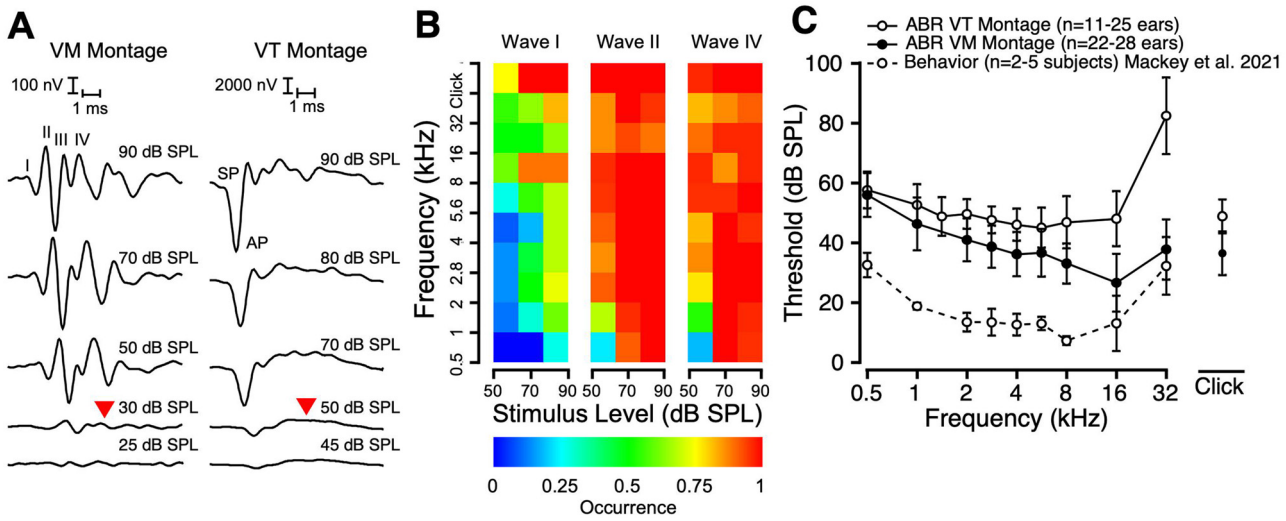

Figure 4. Optimization of ABR electrode montage. A. Exemplar ABR traces using the vertex-to-mastoid electrode montage (VM, left) and the vertex-to-tympanic membrane montage (VT, right). Red triangle depicts the sound level (in dB SPL) at threshold. Waveform components are labeled with roman numerals (I-IV) for the 90-dB SPL VM trace and are labeled with summating potential (SP) and action potential (AP) for the 90-dB SPL VT trace. B. Heatmaps illustrating the probability of occurrence for Wave-I (left), -II (middle), and -IV (right) for all stimuli (clicks and tone bursts: 0.5, 1, 2, 2.8, 4, 5.7, 8, 16, 32 kHz) as a function of presentation level (dB SPL) using the VM electrode montage (n = 22-28 ears). Blue colors depict lower wave occurrence. Red colors depict higher wave occurrence. C. Average threshold (dB SPL) (± 1 SD) as a function of frequency (kHz). Thresholds derived using the VT electrode montage (n = 11-25 ears), the VM electrode montage (n = 22-28 ears), and behavioral thresholds (n = 2-4 ears) interpolated from data in Mackey et al. (2021) are represented with unfilled circles, filled circles, and unfilled circles with a dashed line, respectively. (For interpretation of the references to color in this figure legend, the reader is referred to the web version of this article.)

nents (labeled Waves I-IV in Figure 4A) that decreased in amplitude as stimulus level decreased. The identification of Waves II-IV with the VM electrode, which were not identified with the VT electrode, opportunely allowed for further exploratory analysis of the ABR when using the vertex-to-mastoid montage (e.g., relative wave metrics, inter-wave metrics, etc.), which are discussed in detail in a later section.

The probability of occurrence for Wave-I, -II, and -IV using the VM montage are shown with a heatmap in Figure 4B (blue colors depict lower occurrence and red colors depict higher occurrence for each waveform component). Across all stimuli, Wave-II and Wave-IV were the most identifiable waveform components. At supra-threshold levels, Wave-II had a 93-100% probability of occurring and Wave-IV had a 62-100% probability of occurring (Figure 4B). As sound pressure level decreased down to the level at which threshold was identified, Wave-II was present 48.39% of the time and Wave-IV was present 44.11% of the time. In contrast, Wave-I was the least often detected waveform component and the most strongly impacted by both stimulus level and frequency (see the blue colors depicting lower occurrence in the leftmost heatmap in Figure 4B). At supra-threshold levels, Wave-I was most detectable in response to clicks (75-100% probability of occurring) and least detectable in response to 0.5 kHz tone bursts (0-27% probability of occurring). As sound pressure level decreased down closer to the level at which threshold was identified, Wave-I was only present 4.07% of the time.

3.3.2. Normative ABR thresholds

Average ABR thresholds, as determined by the presence and repeatability of any wave component above the noise floor, are plotted as a function of tone burst frequency in Figure 4C (n = 22-28 ears, VM electrode montage; n = 11-25, VT electrode montage). For all tone burst frequencies, the VM electrode montage produced lower average ABR thresholds compared to the VT electrode montage (compare filled black circles with unfilled circles connected by solid lines in Figure 4C). The smallest difference in average ABR thresholds between electrode montages occurred at 0.5 kHz (2.1 dB difference), and the largest difference occurred at 32 kHz (45.3 dB difference). In general, ABR threshold differences between electrode montages were smaller at lower frequencies (0.5-5.6 kHz), and larger at higher frequencies (8-32 kHz). The higher thresholds for the VT montage, especially for frequencies ≥ 16 kHz, may have occurred because of partial ear canal occlusion, and/or because of the pressure and weight of the electrode gel and ball electrode against the tympanic membrane, thereby altering the tympanic membrane's vibration. Both mechanisms (i.e., occlusion of the ear canal and pressure/weight on the tympanic membrane) have the potential to attenuate the sound energy reaching the cochlea and thus influence the threshold of high frequency sounds.

For the VM electrode montage, the frequency range of greatest sensitivity occurred from 4-16 kHz with the lowest average threshold value at 26.6 dB SPL at 16 kHz (Figure 4C, filled circles connected by solid line). For the VT electrode montage, the area of greatest sensitivity occurred from 1.5-16 kHz with the lowest average threshold value at 45.0 dB SPL at 6 kHz (Figure 4C, unfilled circles connected by solid line). Characteristically, the area of greatest sensitivity for both electrode montages was surrounded on both ends of the tested frequency range with elevated tails: shallow at the low frequency tail and steep at the high frequency tail (Figure 4C).

Compared to behaviorally derived hearing thresholds at 200ms tone durations, a common stimulus duration used in audiology clinics to assess hearing sensitivity, electrophysiologically derived hearing thresholds are elevated by 18 to 46 dB SPL, with an average elevation in threshold of 35 dB SPL across frequencies (Burton et al., 2019; Dylla et al., 2013; Mackey et al., 2021). Given the shorter duration of ABR tone bursts compared to the behavioral tone stimuli used in the clinic (i.e., 1.5-6ms and 200ms, respectively), behaviorally derived hearing thresholds at equivalent tone durations to ABR tone bursts were interpolated from behavioral data obtained from a study of the effect of stimulus duration on behavioral threshold in macaques (Figure 4C, unfilled circles connected by dashed line) Mackey et al. (2021). These data show that when differences in stimulus duration are accounted for, there are still large differences between ABR and behavioral thresholds. This suggests that other mechanisms beyond temporal integration, such

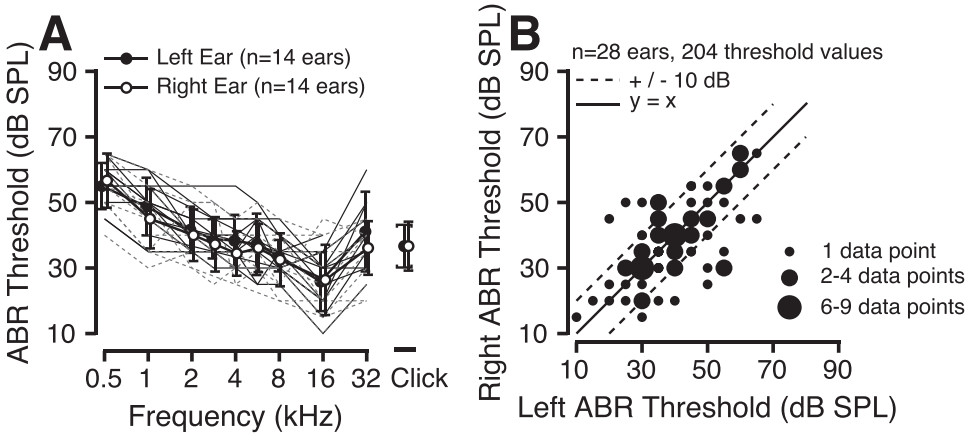

Figure 5. Within-subject comparison of ABR thresholds across ears using the VM electrode montage. A. Average ABR thresholds (dB SPL) (± 1 SD) as a function of stimulus frequency (kHz) for the left ear (n = 14 ears) and the right ear (n = 14 ears). Individual thresholds are shown with dark solid gray lines (left ear) and light dashed gray lines (right ear). B. Scatter plot depicting each subject's right ear ABR threshold (dB SPL) against their left ear ABR threshold (dB SPL) (n = 28 ears, 204 threshold traces) for all stimuli (clicks and tone bursts: 0.5, 1, 2, 2.8, 4, 5.7, 8, 16, 32 kHz). Small, filled circles represent 1 data point. Medium, filled circles represent 2-4 data points. Large, filled circles represent 6-9 data points.

as the higher-level cognitive processes that accompany behavioral task performance, are needed to fully explain threshold differences.

Interaural symmetry of ABR thresholds was evaluated to establish normal across-ear differences and to help guide the identification of asymmetric hearing loss following future experimental manipulations (e.g., noise-induced pathologies). Average right and left ear ABR thresholds are juxtaposed as a function of frequency in Figure 5A (filled circles depict left ear, unfilled circles depict right ear; n = 28 ears). In Figure 5B, right ear thresholds are plotted as a function of left ear thresholds (Figure 5B; n = 28 ears) for ease of identifying threshold asymmetries in the same subjects by observing the degree of deviation of each data point from the X=Y line. Data from all stimuli (clicks and tone bursts) were included in the same plot, resulting in 102 pairs of threshold values (204 individual thresholds). The interaural symmetry data are depicted by filled black circles; the larger the black circle, the more threshold pairs are represented at that XY intersection. Left ear threshold significantly predicted right ear threshold in a linear regression model that took the form "Right Ear Threshold ~ 1 + Left Ear Threshold" (coefficient estimate: 0.65, t = 8.54, p = 1.53e-13). Threshold differences between ears ranged from 0 to 30 dB, with an average interaural threshold difference of 6-dB (SD = 7.02, 95% CI [4.84, 7.60]). 93% of interaural threshold pairs were within +/- 10-dB of each other (see data points within the dashed lines in Figure 5B), and 7% of interaural threshold differences were greater than 10-dB (see data points outside of the dashed lines in Figure 5B). Notably, one subject accounted for 36% of the interaural threshold differences that were greater than 10-dB. According to human clinical norms, which define a significant asymmetry as interaural differences of ≥ 20-dB at any two contiguous frequencies (Durakovic et al., 2019), this subject had a significant threshold asymmetry between ears. No other subjects met, nor exceeded, this symmetry criterion.

In subsequent sections, normative data will be described for the VM electrode montage only. Although the VT electrode montage produced a more robust Wave-I response, the mastoid electrode placement resulted in a more complete ABR morphology with four waveform components (Waves I-IV) and lower ABR thresholds. Further, in terms of translation of these data to human clinical populations, the VM montage more closely mimics human audiologic testing, which typically involves the use of disposable sticker electrodes on the earlobe (A1 and A2) or mastoid (M1 and M2) for reference and ground electrode placement, and Cz for active electrode placement (Crumley, 2011).

3.3.4. Normative ABR latencies

Average latency of ABR Wave-I, -II, and -IV in response to clicks (n = 5-28 ears) and tone bursts (n = 6-28 ears) are shown in Figure 6. Latency of Wave-I, -II, and -IV decreased monotonically as click presentation level increased (Figure 6A). A shorter latency at higher stimulus intensities is consistent with an increased number of neurons responding, an increased neural firing rate, a quicker rise of postsynaptic potentials, and faster synaptic transmission (Picton et al., 1977). On average, for a 90-dB SPL click stimulus, Wave-I latency occurred at 1.1ms (filled black circles), Wave-II latency occurred at 2.2ms (unfilled circles), and Wave-IV latency occurred at 4.0ms (filled gray circles) (Figure 6A). These results are consistent with the average neural conduction times obtained for the Wave I-II inter-wave interval, Wave II-IV inter-wave interval, and Wave I-IV inter-wave interval, which were 1.12ms (SD = 0.14ms), 1.77ms (SD = 0.14ms), and 2.9ms (SD = 0.21ms), respectively. Notably, inter-wave latencies were highly stable as a function of stimulus and presentation level, which can be grossly observed by the consistent ~1ms separation between black and white symbols, and ~1.5ms separation between white and gray symbols across stimulus levels and frequencies in Figures 6A and 6B. For this reason, only the inter-wave latencies for a 90-dB SPL click stimulus were reported in Figure 6A and Figure 7. Histograms for each of the reported inter-wave latencies in response to 90-dB SPL clicks are shown in Figure 7. Notably, there was a very small data range for the Wave I-II latency (Figure 7A), suggesting highly consistent findings across subjects compared to Wave II-IV (Figure 7B) and I-IV (Figure 7C) latencies, which revealed a larger data spread. The 5th, 10th, 50th, 90th, and 95th percentiles for each of the reported inter-wave latencies can be found in Table 2. In response to 90-dB SPL tone bursts (Figure 6B), the latency of Wave-I, -II, and -IV decreased monotonically as tone burst frequency increased, consistent with the known tonotopic organization of the cochlea (Békésy, 1960; Wever, 1949).

Interaural symmetry of ABR latencies was evaluated to establish normal across-ear differences and to help guide the identification of asymmetric hearing loss following future experimental manipulations (e.g., noise-induced pathologies). Individual ear latencies for Wave-I, -II, and -IV are plotted as a function of frequency for 28 macaque ears in Figures 8A (Wave-I), 8C (Wave-II), and 8E (Wave-IV). The dark gray solid lines depict responses obtained from subjects' left ear and the light gray dashed lines depict responses obtained from the subjects' right ear. Intersubject vari-

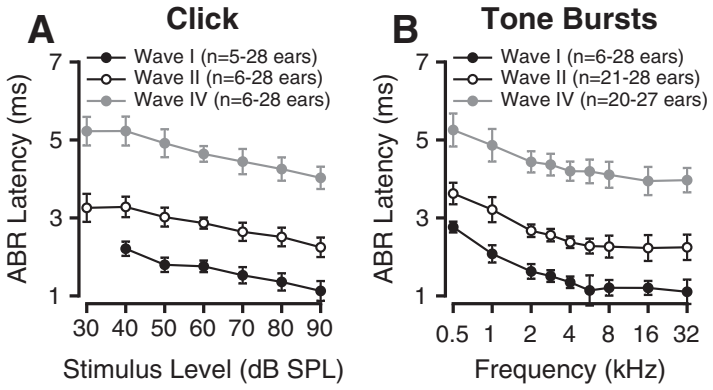

Figure 6. Latency of ABR Wave-I (black circles), -II (open circles), and -IV (gray circles) using the VM electrode montage. A. Average latency (ms) (± 1 SD) of ABR waves as a function of stimulus level (dB SPL) for click stimuli (n = 5-28 ears). B. Average latency (ms) (± 1 SD) of ABR waves as a function of frequency (kHz) in response to a 90-dB SPL stimulus level (n = 6-28 ears).

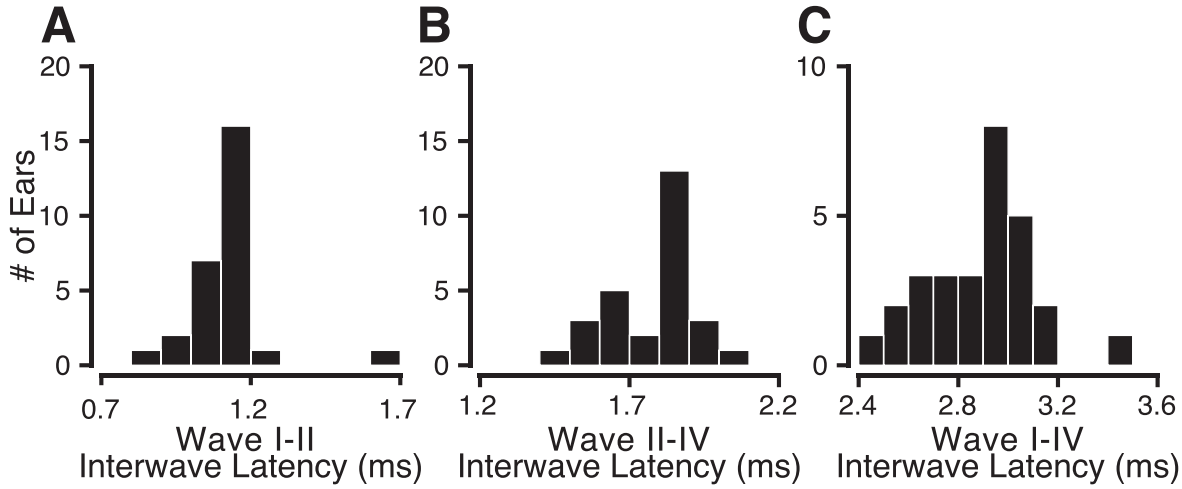

Figure 7. Histograms showing the number of ears (n = 28 ears) as a function of Wave I-II (A), Wave II-IV (B), and Wave I-IV (C) interwave latencies (ms).

Table 2
5th, 10th, 50th, 90th, and 95th Percentiles of intwerwave latencies

	5th Percentile	10th Percentile	50th Prcentile	90th Percentile	95th Percentile
Wave I-II (ms)	0.93	1.00	1.11	1.19	1.28
Wave II-IV (ms)	1.52	1.53	1.81	1.93	1.98
Wave I-IV (ms)	2.54	2.60	2.92	3.1	3.2

Note. ms = milliseconds.

ability was smallest for Wave-I and increased for Wave-II, and -IV (see widening spread of dark and light gray lines from Figure 8A to 8C to 8E, especially at 1 kHz). Interaural symmetry of ABR latencies was evaluated by plotting right ear latency as a function of left ear latency for Wave-I, -II, and -IV using the same 28 macaque ears (Figures 8B, 8D, and 8F). Data from all stimuli were included in the same plot, resulting in 53 pairs (106 individual data points) of Wave-I latency values (Figure 8B), 100 pairs (200 individual data points) of Wave-II latency values (Figure 8D), and 99 pairs (198 individual data points) of Wave-IV latency values (Figure 8F). On average, latency differences between ears were 0.17ms for Wave-I (SD = 0.17, 95% CI [0.12, 0.22]), 0.19ms for Wave-II (SD = 0.21, 95% CI [0.15, 0.23]), and 0.22ms for Wave-IV (SD = 0.23, 95% CI [0.18, 0.27]). 96.2%, 96%, and 95.5% of interaural latency pairs fell within +/- 0.5ms of each other for Wave-I, -II, and -IV, respectively (see data points within the dashed lines in Figure 8B, 8D, and 8F). Left ear latency significantly predicted right ear latency in a linear regression model that took the form "Right Ear Latency ~ 1 + Left Ear Latency" for Wave-I (coefficient estimate: 0.87, t = 12.28, p = 5.43e-17), Wave-II (coefficient estimate: 0.75, t = 17.18, p = 2.51e-31), and Wave-IV (coefficient estimate: 0.84, t = 14.29, p = 1.32e-25). The higher interaural latency differences observed for Wave-II and -IV are consistent with waveform generators that are later/higher in the ascending auditory pathway, thereby causing Wave-II and -IV to incorporate the variability of additional neural conduction components. Further, this result is also consistent with a Poisson process, in which a larger mean (i.e., a larger mean latency for Wave-II and -IV) implies more variability.

3.3.5. Normative ABR amplitudes

Peak-to-trough amplitude of ABR Wave-I, -II, and -IV in response to clicks (n = 4-28 ears) and tone bursts (n = 6-28 ears) are shown in Figure 9A and 9B, respectively. As click presentation level increased, ABR amplitudes generally increased (Figure 9A). As stimulus frequency increased, ABR Wave-I, -II, and -IV amplitudes showed no clear pattern (Figure 9B). Across all click levels (Figure 9A) and frequencies (Figure 9B), ABR Wave-II consistently had the largest amplitude, followed by Wave-IV and Wave-I. This

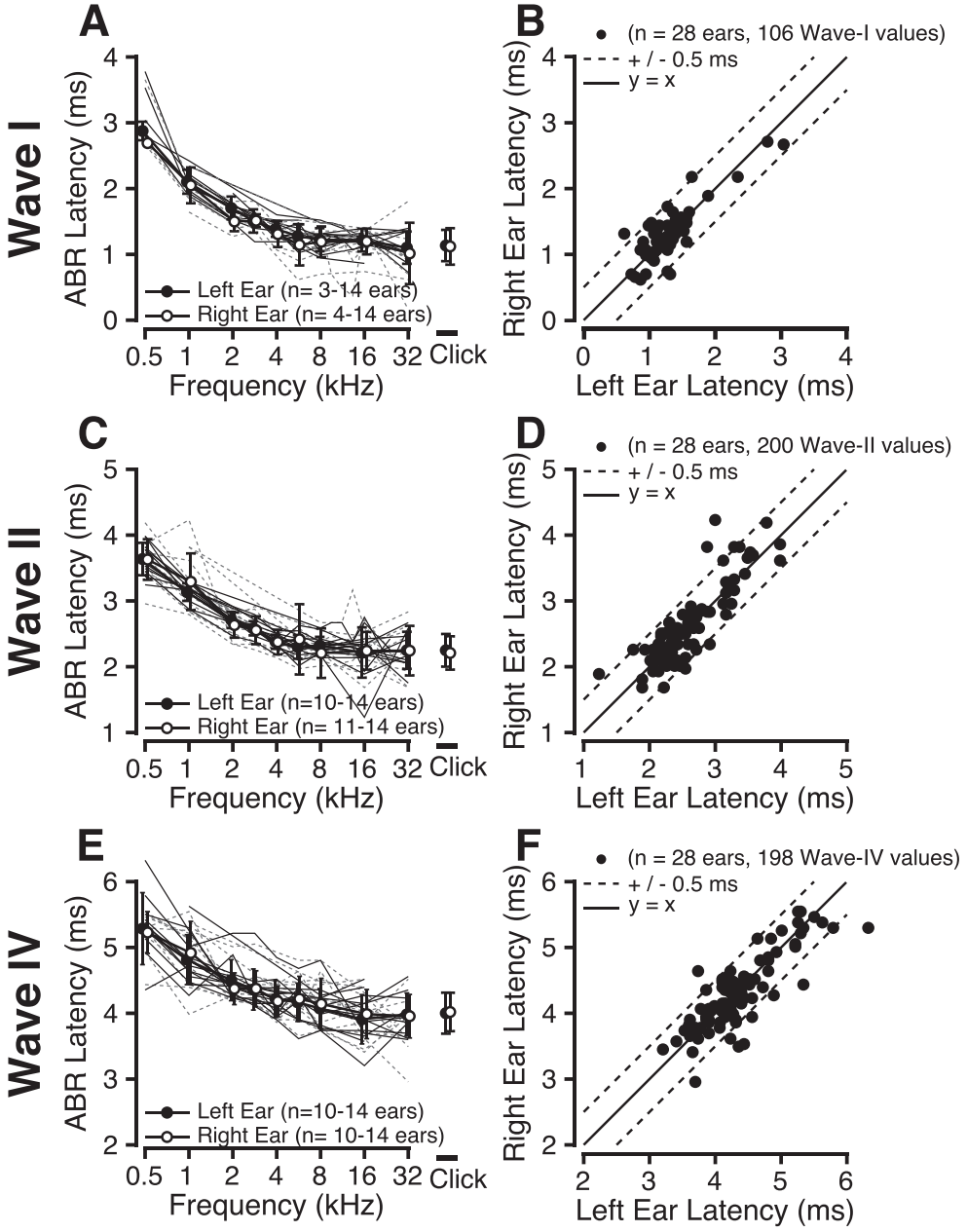

Figure 8. Within-subject comparison of ABR latencies across ears using the VM electrode montage. A, C, E. Average Wave -I (A), -II (C), and -IV (E) latency (ms) (± 1 SD) as a function of stimulus frequency at 90-dB SPL (clicks and tone bursts: 0.5, 1, 2, 2.8, 4, 5.7, 8, 16, 32 kHz). Right ear thresholds depicted by unfilled circles (n = 14 ears). Left ear thresholds are depicted by filled circles (n = 14 ears). Individual ear latencies shown with dark solid gray lines (left ear) and light dashed gray lines (right ear). B, E, F. Scatter plot depicting each subject's right ear latency (ms) against their left ear latency (dB SPL) for Wave-I (B) (n = 28 ears, 106 Wave-I values), -II (D) (n = 28 ears, 200 Wave II values), and -IV (F) (n = 28 ears, 198 Wave II values) for all stimuli at 90-dB SPL (clicks and tone bursts: 0.5, 1, 2, 2.8, 4, 5.7, 8, 16, 32 kHz).

is consistent with the finding that Wave-II and -IV were the most identifiable waveform components down to the level of threshold. On average, the largest click-evoked amplitudes occurred at 80 dB SPL for Wave-I (168.6 nV ± 94.9) and -II (591.7 nV ± 223.6), and at 90 dB SPL for Wave-IV (326.4 nV ± 193.3). In general, tone burst-evoked amplitudes were considerably smaller than click-evoked amplitudes (note the difference in the Y-axis scales for Figures 9A and 9B). Despite differences in raw amplitude values, both click-evoked (Figure 9A) and tone burst-evoked (Figure 9B) ABR amplitudes exhibited considerable inter-subject variability, with the largest variability occurring for Wave-II (SD = 223.6 for an 80-dB SPL click; SD = 233.1 nV for a 90-dB SPL 32 kHz tone burst). This result is consistent with a Poisson process, in which a larger mean (i.e., larger mean amplitude for Wave-II) implies more variability.

3.3.6. Test-retest effects on ABR amplitudes and latencies

Within- (n = 12 ears) and across-session (n = 11 ears) test-retest reliability was assessed for a 90-dB SPL click to examine the normal variability for this measure. Within-session measurements were made during the same procedure, and the electrodes and insert earphone were removed and replaced between Test 1 and Test 2. Across-session measurements were completed during separate procedures that took place approximately 2 weeks to 4 months apart; the speaker was calibrated prior to each test. Examples of waveform traces displaying exemplar and poor within- and across-session test re-test reliability are shown in Figures 10A and 10B, respectively (top: within session, bottom: across session). Test 2 measures are shown as a function of Test 1 measures for amplitude and latency for Wave-I, -II, and -IV in Figures 10C and

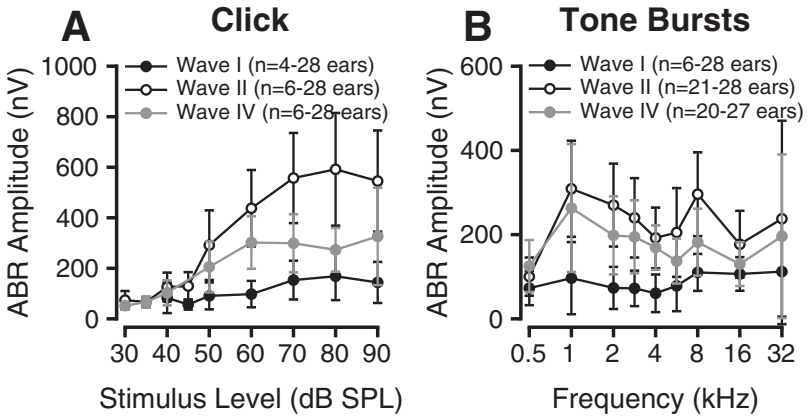

Figure 9. ABR wave amplitudes using the VM electrode montage. A. Average peak-to-trough amplitude (nV) (± 1 SD) of ABR Wave-I (filled black circles), -II (unfilled squares), and -IV (filled gray circles) as a function of stimulus level (dB SPL) for click stimuli (n = 4-28 ears). B. Average peak-to-trough amplitude (nV) (± 1 SD) of ABR Wave-I (filled black circles), -II (unfilled squares), and -IV (filled gray circles) as a function of frequency (kHz) for 90-dB SPL tone burst stimuli (n = 5-28 ears).

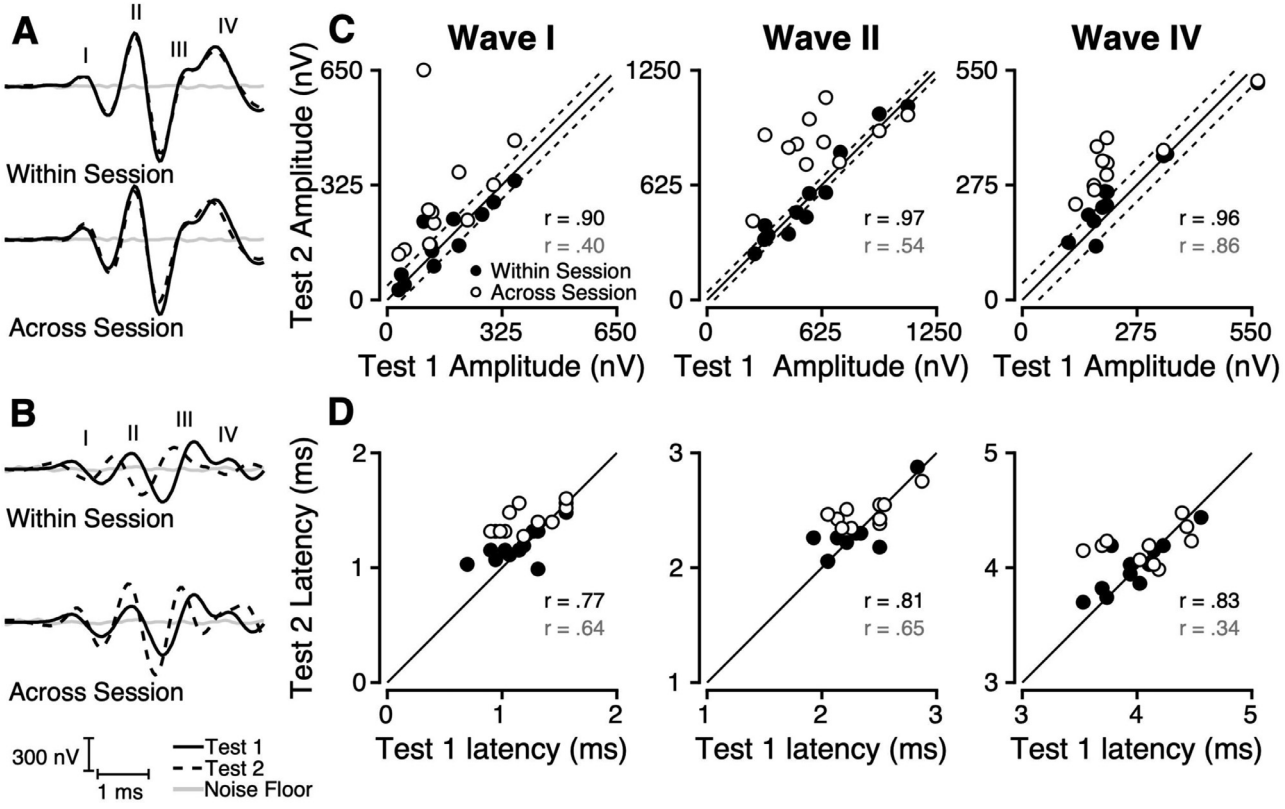

Figure 10. Within- and across-session test-retest reliability for a 90-dB SPL click stimulus using the VM electrode montage. A. Exemplar within- (n = 9 ears) and across- (n = 2 ears) session test-retest reliability. Within-session (top) Test 1 (solid line) and Test 2 (dashed line), and across-session (bottom) Test 1 (solid line) and Test 2 (dashed line) are from the same subject and ear. B. Poor within- (n = 3 ears) and across- (n = 9 ears) session test-retest reliability. Within-session (top) Test 1 (solid line) and Test 2 (dashed line), and across-session (bottom) Test 1 (solid line) and Test 2 (dashed line) are from the same subject and ear, but from a different subject than shown in 8A. C. Test 2 amplitude (nV) as a function of Test 1 amplitude (nV) for Wave-I (left), -II (middle), and -IV (right). Unfilled circles are from the same subject, ear, and test session (n = 12 ears). Filled circles are from the same subject and ear, but different test sessions (n = 11 ears). Spearman correlation coefficients (r) are reported as a summary statistic (black text represents within-session coefficient; gray text represents across-session coefficient). D. Test 2 latency (ms) as a function of Test 1 latency (ms) for Wave-I (left), -II (middle), and -IV (right). Unfilled circles are from the same subject, ear, and test session (n = 12 ears). Filled circles are from the same subject and ear, but different test sessions (n = 11 ears). Spearman correlation coefficients (r) are reported as a summary statistic (black text represents within-session coefficient; gray text represents across-session coefficient).

10D, respectively. The y = x line (diagonal) represents equal Test 1 and Test 2 measures, and thus perfect reliability of measurement. The dashed lines in the amplitude figures (Figure 10C) represent the average noise floor of the recording sessions (± 40 nV). The filled circles represent test-retest data points collected within a recording session (within-session) and the unfilled circles represent across-session data points. Qualitatively, in the amplitude figures (Figure 10C), the across-session data points (unfilled circles) deviated further from the y = x line compared to the within-session data points (filled circles), suggesting poorer test-retest reliability across-sessions compared to within-sessions. Further, the across-session data points also deviated further from the dashed lines, suggesting variability in amplitude beyond what was expected from the noise floor of the recording sessions. In the la-

Table 3
Within- and across-session ICC values for test-retest reliability of ABR wave amplitudes and latencies using the VM electrode montage

	Amplitude		
	Wave-I	Wave-II	Wave-IV
Within Session	0.90 [0.72, 0.97]	0.97 [0.92, 0.99]	0.95 [0.84, 0.99]
Across Session	0.14 [-0.46, 0.66]	0.16 [-0.44, 0.67]	0.44 [-0.16, 0.81]
	Latency		
	Wave-I	Wave-II	Wave-IV
Within Session	0.73 [0.32, 0.91]	0.82 [0.50, 0.94]	0.82 [0.47, 0.95]
Across Session	0.16 [-0.44, 0.67]	0.39 [-0.21, 0.79]	0.23 [-0.38, 0.71]

Note. Intraclass correlation (ICC) values reported here are ICC1 values as defined by Shrout and Fleiss (1979). Lower and upper 95% confidence intervals are shown in brackets.

tency figures (Figure 10D), similar trends can be seen, but the differences in deviations between the filled and unfilled circles were slightly less pronounced, especially for Wave-I.

The Spearman correlation coefficient (r) was used as a descriptive summary statistic of the Test 2 vs. Test 1 amplitude and latency relationships. For both amplitude and latency, correlation coefficients were larger for within-session than across-session test-retest reliability (compare black and gray r values in Figure 10C and 10D; black text represents within-session, gray text represents across-session). This finding suggests that within-session test-retest reliability is greater (i.e., better) than across-session test-retest reliability for both amplitude and latency. To quantify the reliability of the amplitude and latency measures more formally, the intraclass correlation coefficient (ICC1) was used (similar to Prendergast et al., 2018). ICC1 values are shown with 95% confidence intervals in Table 3. ICC1s were largest for within-session Wave-I, -II, and -IV amplitude and within-session Wave-II and -IV latency. These ICC1 values were >0.75, suggesting excellent repeatability (Cicchetti, 1994). The within-session Wave-I latency ICC1 value fell just outside of this criteria, and instead would be considered good repeatability (Cicchetti, 1994). ICC1s were lowest for across-session Wave-I, -II, and -IV amplitude and latency and are considered poor repeatability (Cicchetti, 1994).

3.3.7. Normative ABR amplitude ratios

Due to the high variability of Wave-I amplitudes found in humans (Lauter and Loomis, 1988), Wave-V amplitude, which appears to be less affected by deafferentation in the auditory periphery, has been suggested as a normalization denominator (Bharadwaj et al., 2019). Here, macaque Wave-IV, which is thought to be homologous to human Wave-V (Kraus et al., 1985), was used in the denominator as a normalization factor. Wave-I/IV and Wave-II/IV amplitude ratios in response to clicks (n = 15-28 ears) and tone bursts (n = 6-27 ears) are shown in Figure 11. Consistent with the raw Wave -I, -II, and -IV amplitudes shown in Figure 9, mean Wave-I/IV amplitude ratios (filled circles) were < 1 (range: 0.36 to 0.96 for 90-dB SPL tone bursts), indicating Wave-I was smaller than Wave-IV (see that the filled circles are below the dashed y = 1 line in Figure 11A, 11B). Mean Wave -II/IV amplitude ratios (unfilled circles) were > 1 (range: 1.06 to 1.86 for 90-dB SPL tone bursts), indicating Wave-II amplitudes were larger than Wave-IV (see that the unfilled circles are above the dashed y = 1 line in Figure 11A, 11B). These trends were observed for all stimuli, regardless of intensity (Figure 11A) or frequency (Figure 11B). Also consistent with the raw Wave I-IV amplitudes, Wave-II/IV amplitude ratios had greater variability compared to Wave-I/IV amplitude ratios (Figure 11A, 11B), mimicking the greater mean and variability observed in the raw amplitudes of Wave-II and -IV compared to Wave-I (Figure 9).

3.3.8. Effects of stimulus rate on ABR amplitudes and latencies

Temporal resolution is thought to be impaired in some forms of subclinical cochlear pathologies (Lee et al., 2021; Shi et al., 2016; Song et al., 2016). To create a normative data set in macaques, adaptation and temporal resolution were assessed using two metrics: single suprathreshold clicks with varying presentation rates (27.7/s, 57.7/s, 100/s, 125/s, 166.6/s, 200/s) (exemplar responses shown in Figure 12A) and paired suprathreshold clicks with varying inter-click intervals (10, 8, 4, 2, 1ms) (exemplar responses in Figure 13A).

Amplitudes and latencies of Wave-I, -II, and -IV as a function of 90 dB SPL click presentation rate are shown in Figure 12 (n = 22-23 ears). As click rate increased from 27.7/s to 200/s, the amplitude of Waves I-IV decreased (Figure 12B), and latency increased (Figure 12C), consistent with the exemplar in Figure 12A. Of note, the effect of a 200/s click rate on Wave-IV amplitude and latency could not be assessed due to limitations of the recording window (see the shorter 200/s trace in black in Figure 12A). Similar trends of decreasing amplitude and increasing latency as a function of increasing click presentation rate for Wave-I, -II, and -IV were observed for 80- and 70-dB SPL clicks (data not shown).

The second way of assessing temporal resolution and adaptation used two clicks presented with interclick intervals ranging from 1 – 10 ms, with the first click of the pair being presented every 36.1 ms (27.7/s presentation rate) (red triangles in Figure 13A depict when the clicks were presented). At longer interclick intervals (8 - 10 ms), the response to the two clicks were separate and apparent (Figure 13A). However, at ICIs less than 8 ms, the response to the Click 1 overlapped with the response to Click 2 (Figure 13A). To assess the response to Click 2 in those cases, we subtracted the response to the single click at 27.7/s presentation rate to zero out (i.e., remove) the response to Click 1 and estimate the response to Click 2 alone (examples of traces after subtraction are shown in the black outlined box Figure 13A). Amplitudes and latencies of Wave-I, -II, and -IV in response to Click 2 as a function of increasing 90 dB SPL click pair ICI are shown in Figure 13B and 13C (n = 22-23 ears). As ICI increased from 1 to 10ms, the amplitude of the Click 2 response increased for Wave-I and -II, whereas the amplitude of the Click 2 response for Wave-IV generally displayed an increase from 1 to 4ms followed by a decrease from 4 to 10ms (Figure 13B). As ICI increased from 1 to 10ms, the latency of the Wave-I of the Click 2 response remained relatively unchanged (1.11ms at 1ms ICI, 1.18ms at 10ms ICI), whereas the latency of Wave-II of the Click 2 response increased slightly (2.24ms at 1ms ICI, 2.36ms at 10ms ICI), and the latency of Wave-IV of the Click 2 response more apparently increased with increasing ICI (3.64ms at 1ms ICI, 3.92 at 10ms ICI) (Figure 13C). Similar trends were observed for 80- and 70-dB SPL click pairs (data not shown).

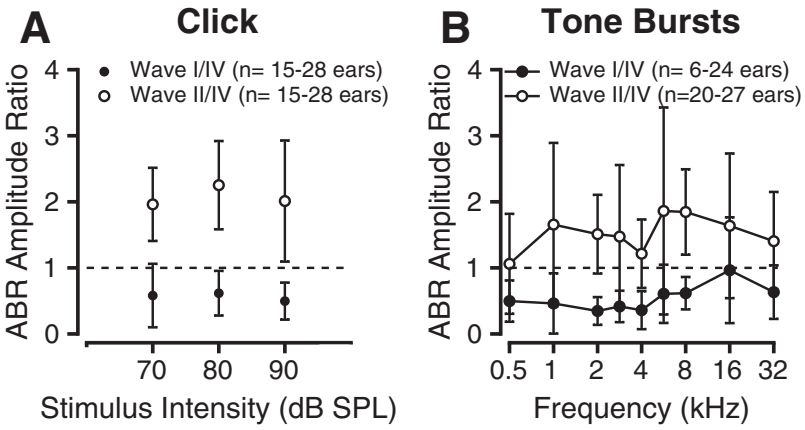

Figure 11. ABR wave amplitude ratios using the VM electrode montage. A. Average amplitude ratio (± 1 SD) as a function of stimulus level (dB SPL) for click stimuli. Wave I/IV amplitude depicted by filled black circles (n = 15-28 ears). Wave II/IV amplitude depicted by unfilled circles (n = 15-28 ears). B. Average amplitude ratios (± 1 SD) as a function of stimulus frequency (kHz) for 90 dB SPL tone burst stimuli. Wave I/IV amplitude depicted by filled circles (n = 6-24 ears). Wave II/IV amplitude depicted by unfilled circles (n = 20-27 ears).

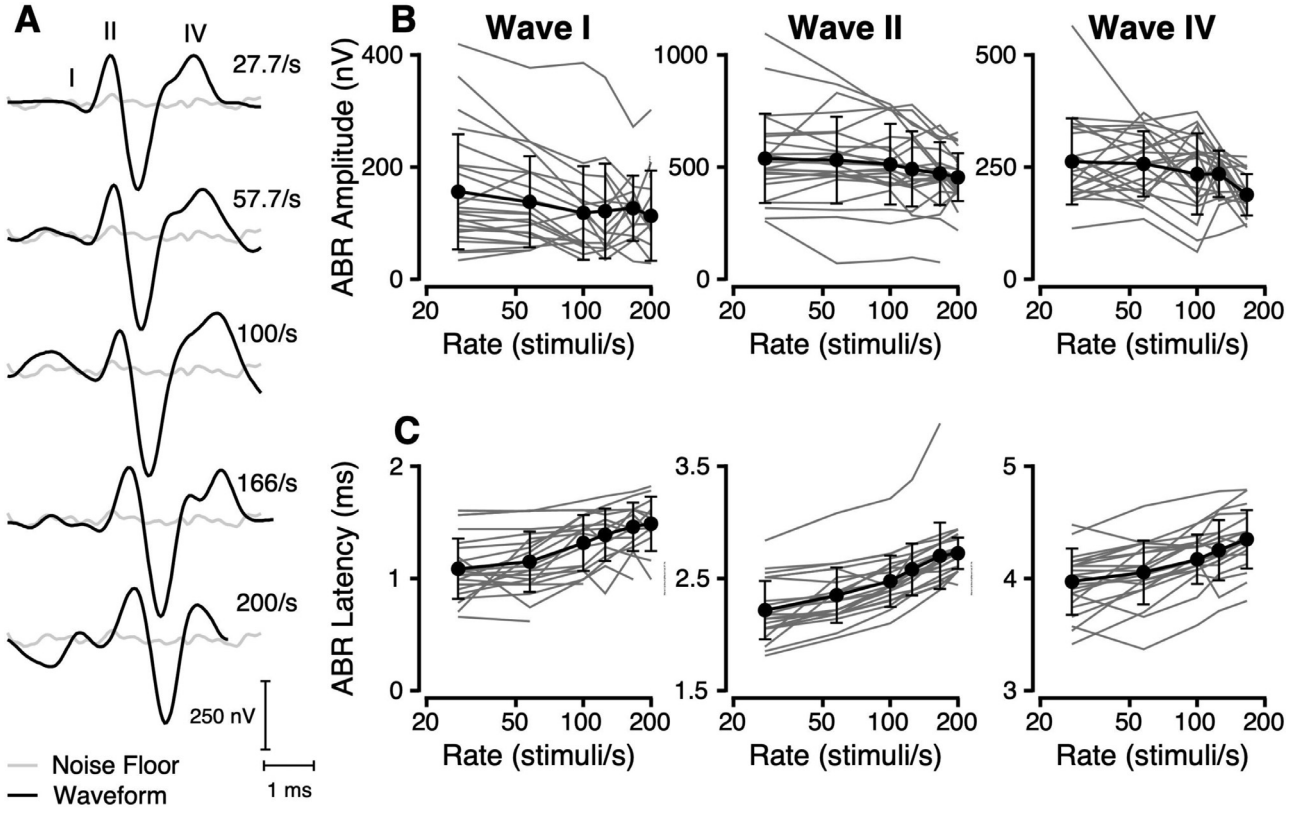

Figure 12. Effect of click presentation rate on ABR wave amplitude and latency using the VM montage. A. Example traces from the same subject and same ear in response to 90-dB SPL clicks presented at 27.7/s, 57.7/s. 100/s, 166.6/s, and 200/s (from top to bottom, respectively). Light gray lines display the noise floor of the recording. B. Average ABR amplitude (nV) (± 1 SD) in response to 90-dB SPL clicks as a function of presentation rate (stimuli/second) for Wave-I (left), -II (middle), and -IV (right) (n= 22-23 ears). Light gray lines represent individual ears. C. Average ABR latency (ms) (± 1 SD) in response to 90-dB SPL clicks as a function of presentation rate (stimuli/second) for Wave-I (left), -II (middle), and -IV (right) (n= 22-23 ears). Light gray lines represent individual ears.

4. Discussion

DPOAEs and ABRs are well-established diagnostic tools widely used in audiology clinics to physiologically assess auditory function. DPOAE amplitudes, ABR thresholds, and ABR Wave-V latencies remain the most obtained metrics of these measures. However, clinically novel metrics and stimuli continue to be investigated as potential candidate diagnostic tools of subclinical pathologies (e.g., DPOAE thresholds, ABR amplitudes, ABR amplitude ratios, and ABRs in response to single clicks with varying presentation rates and click pairs with varying inter-click intervals) and for metrics of location-specific damage. Here, we established normative values for these clinically traditional and novel metrics and stimuli in a large cohort of male macaque monkeys.

4.1. Distortion product otoacoustic emissions (DPOAEs)

DPOAEs are arguably one of the audiometric tools with the highest diagnostic specificity as they are intimately linked to the operating characteristics and the gross integrity of cochlear outer

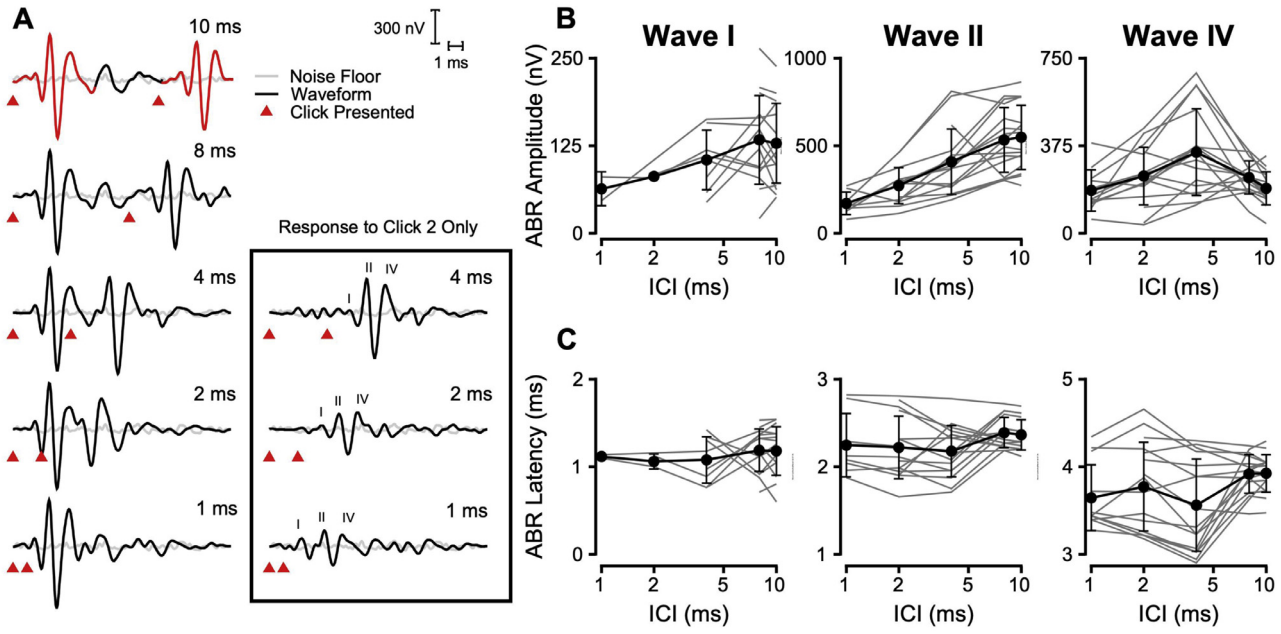

Figure 13. ABR wave amplitudes and latencies in response to click pairs of varying inter-click intervals using the VM electrode montage. A. Example traces from the same subject and same ear in response to 90-dB SPL clicks pairs with 10, 8, 4, 2, and 1 ms ICIs (from top to bottom, respectively). Light gray lines display the noise floor of the recording. The 3 traces outlined with a black box are the same traces shown for 4, 2, and 1 ms ICIs. However, the response to Click 1 was subtracted from the waveform trace to isolate the response to Click 2. This was accomplished by subtracting a trace in response to a single click at a 27.7/s presentation rate for the same subject ear, and sound level (as described in further detail in Lee et al., 2020). B. Average ABR wave amplitude (nV) in response to Click 2 (± 1 SD) as a function of inter-click interval (ICI; ms) for Wave-I (left), -II (middle), and -IV (right). Light gray lines represent individual ears. C. Average ABR wave latency (ms) in response to Click 2 (± 1 SD) as a function of inter-click interval (ICI; ms) for Wave-I (left), -II (middle), and -IV (right). Light gray lines represent individual ears. (For interpretation of the references to color in this figure legend, the reader is referred to the web version of this article.)

hair cells (OHCs) (Lonsbury-Martin and Martin, 1990). In the clinic, DPOAEs are often performed using a single set of parameters (f_2/f_1 = 1.22; L_1/L_2 = 65/55) (Gorga et al., 1993) to rule out or confirm abnormal OHC function. Notably, because middle ear dysfunction can also result in the absence of OAEs (Wada et al., 1995), tympanometry is critical for the interpretation of DPOAE testing. Here, we sought to identify the optimal stimulus parameters to obtain the most robust DPOAE amplitudes in a cohort of otologically normal macaque monkeys. Then, using these optimal stimulus parameters, we reported two traditional measures of DPOAEs: amplitude and signal-to-noise ratios, and two clinically novel measures of DPOAEs: input-output functions, and threshold.

DPOAE amplitudes and signal-to-noise ratios are measured in the clinic to classify whether a DPOAE response is present or absent. Most clinics classify a DPOAE response as present if the response has at least a 3-6 dB signal-to-noise ratio and a response amplitude that is considered normal in accordance with the patient's age (typically 0 to 25 dB SPL) (Abdala and Visser-Dumont, 2001). In the present study, average DPOAE amplitudes increased as a function of frequency from -5 dB SPL at 0.5 kHz and plateaued at an average level of 15 dB SPL for f_2 frequencies between 3-10 kHz. Similar DP magnitudes have been observed for this frequency range in previous macaque studies (-5 to 15 dB SPL from 1-8 kHz) (Lasky et al., 1995b; Park et al., 1995; Torre and Fowler, 2000), as well as in other species, including mice (-5 to 10 dB SPL up to 6.3 kHz) (Martin et al., 2007), guinea pigs (5-15 dB SPL from 1-3 kHz and 10-20 dB SPL from 4-8 kHz) (Chang and Norton, 1996), and humans (10-30 dB SPL from 0.7-6 kHz) (Marco et al., 1995). Notably, DPOAE amplitudes reported here revealed small within-session (0.25-5.78 dB for L_1= 65 dB SPL) and across-session (2.04-6.81 dB for L_1= 65 dB SPL) test-retest differences, which closely resembled those found in marmoset monkeys for within-session (0.15-5.3 dB for L_1= 50 dB SPL and 0.15-3.4 dB SPL for L_1 = 74 dB SPL) and across-session DPOAE amplitudes (0.12-4.9 dB SPL for L_1 = 74 dB SPL) (Valero and Ratnam, 2011). In humans, standard error of measurement (SEM) values are typically reported for within-session (M= 2.64 dB SPL) and across-session (2.59-3.04 dB SPL) measurements (Ng and Mcpherson, 2005), which resembled average SEM values obtained here (0.15-2.11 dB for within-session, 0.47-2.54 dB for across-session).

DPOAE input-output functions and thresholds are not typically measured in the clinic. However, they are often usen in human and animal research because they may be a more sensitive metric of OHC function, or have a greater relation to behavioral thresholds than DPOAE amplitudes or signal-to-noise ratios derived from high primary tone levels (Boege and Janssen, 2002; Kummer et al., 1998). Here, DPOAE input-output functions increased monotonically with increasing L_2 level across all f_2 frequencies, consistent with data in previous studies in macaques (Lasky et al., 1995b; Lasky et al., 1999; Park et al., 1995), rodents (Shaffer and Long, 2004), and humans (Bonfils et al., 1992; Lasky et al., 1995b). Input-output function slopes were comparable across subjects and f_2 frequencies, similar to the low slope variability reported in previous macaque studies (Lasky et al., 1995b; Lasky et al., 1999) and in humans (Bonfils et al., 1992; Lasky et al., 1995b). Notably, Lasky et al. (1995b) who examined both macaque and human DPOAEs, reported a species difference in DPOAE input-output function slope between macaques and humans, especially at and above 8 kHz, which likely reflects differences in the audible frequency range of the two species. Our macaque DPOAE thresholds displayed a similar U-shape as seen in rats (Shaffer and Long, 2004), mice (Qin et al., 2010; Zehnder et al., 2006), and guinea pigs (Furman et al., 2013; Lin et al., 2011; Pienkowski and Ulfendahl, 2011). The lowest thresholds occurred from 2-10 kHz, consistent with previous reports in macaques (Lasky et al., 1999) and the range of frequencies eliciting the greatest supra-threshold DP amplitudes.

4.2. Auditory brainstem responses (ABRs)

ABRs can be used to screen for grossly normal peripheral auditory function (Norton et al., 2000) and to more specifically estimate type, degree, and configuration of hearing loss (Stapells and Oates, 1997). In conjunction with DPOAEs, ABRs can aid in differential diagnosis by localizing pathology to OHC, or IHC/neuronal dysfunction (Rance et al., 1999; Starr, 1976). Here, we compared ABRs measured with two electrode montages (vertex-to-tympanic membrane and vertex-to-mastoid) to assess which montage resulted in the most robust waveform morphology and amplitudes in a cohort of otologically normal macaque monkeys. Using the more optimal vertex-to-mastoid montage, we established normative datasets for two traditional measures of ABRs: thresholds (determined by the presence of any wave component) and latencies, two clinically novel measures of ABRs: peak-to-trough amplitudes and peak-to-trough amplitude ratios, and two clinically novel ABR stimulus paradigms: single clicks with varying presentation rates and click pairs with varying inter-click intervals.

Our data using the VM montage are consistent with an abundance of findings in prior human literature showing that the amplitude of Wave-I, when recorded with the active electrode on the surface of the scalp, is among the first component to disappear in normal hearing subjects as stimulus intensity is lowered (Fria, 1980; Rowe III, 1978; Schwartz and Berry, 1985). In hearing-impaired subjects, Wave-I may be reduced, distorted, or absent to begin with, despite the presence of a typically identifiable Wave-V (Cashman and Rossman, 1983; Hyde and Blair, 1981). Similarly, in macaques, Wave-I is smaller and more variable compared to Wave-II and Wave-IV (Engle et al., 2014). The VM electrode montage produced a less robust Wave-I amplitude than the VT montage but revealed a more complete ABR morphology with four waveform components (Waves I-IV). This morphology is consistent with other studies in macaque monkeys, which have reported four to five waveform components of the ABR (Allen and Starr, 1978; Doyle et al., 1983; Fria et al., 1982; Lasky et al., 1995a; Ng et al., 2015). Wave-II and -IV were the most detected components, whereas Wave-I was less often detected, similar to previous findings in macaques (Allen and Starr, 1978; Doyle et al., 1983; Lasky et al., 1995a; Ng et al., 2015) and other nonhuman primates (Kraus et al., 1985). In humans, Wave-V is the most robust component, and is used to estimate hearing threshold (Hecox and Galambos, 1974; Sininger, 1993). Wave-I, -II, and -IV in macaques are thought to be homologous to human Wave-I/II, -III, and -V, with loosely associated neural generators of the auditory nerve, cochlear nucleus, and lateral lemniscus, respectively (Lasky et al., 1995a). However, the more widely accepted view is that each ABR waveform component likely represents activity from more than one neural generator due to the far-field nature of these potentials, and the presence of feedforward, feedback, and local micro-circuitry in the auditory brainstem (Allen and Starr, 1978). Because of this, the exact generators of each waveform component and how they relate to the variable ABR morphology across species is largely uncertain.

The vertex-to-mastoid thresholds obtained here are roughly consistent with the macaque ABR thresholds reported by Lasky et al. (1999), and nearly identical to the click ABR thresholds in humans reported by Sininger et al. (1997), but are ~20-dB SPL higher than the human ABR thresholds from 0.5-8 kHz reported by Sininger (1993). The latencies obtained in the present study are consistent with latencies obtained in previous studies in macaques (Allen and Starr, 1978; Doyle et al., 1983) and humans for homologous waves (Gorga et al., 1988; Gorga et al., 1987; Hecox and Galambos, 1974). The similarity between macaque and human ABR latencies, in contrast to smaller mammals, is likely due to the more comparable sizes of macaque and human heads, cochleae, and mechanical and neural pathways (Chambers et al., 1989; Conti et al., 1988; Mitchell et al., 1989; Trune et al., 1988). Notably, because of this similarity between macaque and human ABR latencies, if the macaque generator for Wave-IV is truly analogous to that of human Wave-V, the neural conduction time between the eighth nerve and the generators of these waves is shorter in macaques (2.9ms) than in humans (4ms; Davis, 1976; Galambos and Hecox, 1977) by approximately 1ms. Perhaps this difference could be explained by a difference in auditory brainstem pathway length. Although macaque brains are more comparable to humans than smaller animal models, the brain of humans is still thought to be 4.8 times the size for a hypothetical monkey of the same body weight (Passingham, 2009). Most of this discrepancy is suggested to be a difference in neocortex size (Rilling and Insel, 1999). However, perhaps there is discrepancy (albeit likely more minor) in the size of subcortical structures.

ABR amplitudes and amplitude ratios are not typically measured in the clinic but are known to be affected in certain auditory pathologies, including cases of auditory neuropathy (Starr et al., 1996; Starr et al., 2001), endolymphatic hydrops (Ferraro and Tibbils, 1999; Huang et al., 2011), and mouse models of SYN (Kujawa and Liberman, 2009; Sergeyenko et al., 2013). Compared to smaller mammals, such as rodents (Alvarado et al., 2012; Zhou et al., 2006) and cats (Walsh et al., 1986), the ABR amplitudes reported here and in previous macaque (Ng et al., 2015) and human studies (Prendergast et al., 2018) are smaller in magnitude. This is consistent with the known inverse relation between head size and magnitude of ABR wave amplitudes (Trune et al., 1988). Wave-I/IV amplitude ratios reported here were < 1, indicating a smaller Wave-I compared to Wave-IV, mimicking the reciprocal findings reported in humans for Wave-V/I ratios (Musiek et al., 1984). When electrodes and stimulus parameters are used that are designed to enhance Wave-I responses (e.g., ear canal electrodes and a 7.7/s presentation rate), the Wave-I/V ratio has been reported to be > 1 in humans (Grose et al., 2017). Importantly, the between-subjects variability for amplitudes and amplitude ratios, as well as the within-subjects across-session variability for amplitudes, mimic the large nonpathological variability observed in humans (Don et al., 1993, 1994; Mitchell et al., 1989; Sohmer and Feinmesser, 1967; Stockard et al., 1978; Trune et al., 1988), thus calling into question the diagnostic and translatable capabilities of these metrics. To be a viable clinical tool, the measure of interest must capture pathological variations in peripheral physiology over and beyond the variance that is imposed by non-pathological extraneous variables.

The “poor” repeatability observed for across-session amplitude and latency measurements compared to the “excellent” repeatability observed for within-session amplitude and latency measurements (as classified by criteria in Cicchetti, 1994) (except for within-session Wave-I latency, which was “good” as opposed to “excellent” repeatability) calls into question the diagnostic capabilities of these metrics for long-term patient follow-up on an individual level. To be a viable clinical tool, the measurement of interest must be sensitive enough to track pathological variations within the same individual over time. These variations must exceed the variance that is imposed by non-pathological extraneous variables when re-administering the test. This is accomplished with a measure that has “excellent” across-session test-retest reliability. Here, for both within-and across-session measurements, the insert earphones were removed and reinserted, the electrodes were removed and replaced, and recording equipment (e.g., preamplifier) was turned off and back on. Further, the short time between Test 1 and Test 2 for across-session measurements (2 weeks to 4 months) rules out contributions from age-related pathology. Thus, the non-pathological extraneous variables that are causing the “poor” test-rest reliability in across-session measurements (but not within-session) are outside of the test administrator’s control

(e.g., ambient electrical noise, neurophysiologic noise, anesthesia effects), and would be difficult to ameliorate.

ABR paradigms assessing neural adaptation and recovery from neural adaptation can provide neuro-diagnostic information for in lieu of, or prior to, imaging of the head for retro-cochlear pathology (e.g., MRI, CT) (Daly et al., 1977; Don et al., 1977; Stockard et al., 1977; Tanaka et al., 1996). These ABR paradigms typically consist of two identical stimuli (a masker and the signal of interest) that are presented in increasing (or decreasing) temporal proximity to determine the point at which forward masking occurs (or ceases). Three forward masking stimulus designs have been reported in the literature: i) tone burst-on-tone burst designs (humans: Walton et al., 1999); ii) click-on-click designs (chickens: Burkard et al., 1994; cats: Burkard et al., 1996; gerbils: Burkard and Voigt, 1989; humans: Burkard and Sims, 2001; Skoe and Tufts, 2018); iii) and click pair designs in which the instantaneous rate, rather than the presentation rate, is manipulated (song birds: Henry et al., 2011; rats: Lee et al., 2020; humans: Ohashi et al., 2005; cats: Parham et al., 1998; guinea pigs: Song et al., 2016; dolphins: Supin and Popov, 1995; fish: Wysocki and Ladich, 2002). Here, click-on-click and click pair designs were implemented. As a function of increasing click-on-click presentation rate, amplitudes of all waves decreased and latencies increased, suggesting gradually increasing neural adaptation to the click stimulus, similar to observations in humans (Burkard and Sims, 2001; Skoe and Tufts, 2018) and other species (chickens: Burkard et al., 1994; cats: Burkard et al., 1996; gerbils: Burkard and Voigt, 1989). In contrast, as a function of increasing click pair inter-click-interval (ICI), amplitudes of Wave-I and -II in response to Click 2 increased, suggesting a gradual recovery from neural adaptation, similar to paired click data from dolphins (Supin and Popov, 1995) and studies that reported increasing normalized Click 2 amplitudes (re: amplitude for a single click) with increasing ICI (song birds: Henry et al., 2011; humans: Ohashi et al., 2005; cats: Parham et al., 1998; fish: Wysocki and Ladich, 2002).

5. Conclusion

By establishing a normative data set of traditional and clinically novel physiological measures and stimuli in young, normal hearing macaques, this report i) expands on the existing literature of normative clinical physiological data in nonhuman primates, ii) lays the groundwork for future studies investigating the effects of pathologies (including subclinical noise-induced pathologies) in the macaque model, and iii) contributes to the development of an improved audiological test battery for enhanced differential diagnosis and treatment of human auditory pathologies. The comparison of these measures across different pathologies may reveal the utility of these measures beyond the subclinical cochlear pathologies that have been reported thus far.

6. Author Statement

All authors certify that they have read and approved the version of the document to be submitted.

All authors also declare that they have no conflicts of interest.

Acknolwedgements

The authors would like to thank Mary Feurtado for assistance with all procedures involving anesthesia. The authors would like to thank Jessica Feller, Alex Tarabillo, Namrata Temghare, Rachel Archer, and Samantha Hauser for assistance with data collection. The authors would also like to acknowledge the National Institute on Deafness and Other Communication Disorders of the National Institutes of Health for funding this research through the following grant support: R01 DC 015988 (MPI: R. Ramachandran and B. Shinn-Cunningham) and F32 DC 019817 (PI: J. Burton).

Supplementary materials

Supplementary material associated with this article can be found, in the online version, at doi:10.1016/j.heares.2022.108568.

References

Abdala, C., Visser-Dumont, L., 2001. Distortion product otoacoustic emissions: a tool for hearing assessment and scientific study. The Volta Review 103 (4), 281.

Allen, A.R., Starr, A., 1978. Auditory brain stem potentials in monkey (M. mulatta) and man. Electroencephalogr Clin Neurophysiol 45 (1), 53–63. doi:10.1016/0013-4694(78)90341-3.

Alvarado, J.C., Fuentes-Santamaría, V., Jareño-Flores, T., Blanco, J.L., Juiz, J.M., 2012. Normal variations in the morphology of auditory brainstem response (ABR) waveforms: a study in Wistar rats. Neuroscience research 73 (4), 302–311.

Anderson, H., Barr, B., Wedenberg, E., 1969. Intra-aural reflexes in retrocochlear lesions, Nobel symposium 49–55.

Békésy, G.v., 1960. Vibratory pattern of the basilar membrane. Experiment in Hearing 404–429.

Bharadwaj, H.M., Mai, A.R., Simpson, J.M., Choi, I., Heinz, M.G., Shinn-Cunningham, B.G., 2019. Non-Invasive Assays of Cochlear Synaptopathy–Candidates and Considerations. Neuroscience 407, 53–66.

Boege, P., Janssen, T., 2002. Pure-tone threshold estimation from extrapolated distortion product otoacoustic emission I/O-functions in normal and cochlear hearing loss ears. The Journal of the Acoustical Society of America 111 (4), 1810–1818.

Bonfils, P., Avan, P., Francois, M., Trotoux, J., Narcy, P., 1992. Distortion-product otoacoustic emissions in neonates: normative data. Acta oto-laryngologica 112 (5), 739–744.

Boston, J.R., 1981. Spectra of auditory brainstem responses and spontaneous EEG. IEEE Transactions on Biomedical Engineering (4) 334–341.

Buchwald, J.S., Huang, C., 1975. Far-field acoustic response: origins in the cat. Science 189 (4200), 382–384. doi:10.1126/science.1145206.

Burkard, R., Jones, S., Jones, T., 1994. Conventional and cross-correlation brain-stem auditory-evoked responses in the white leghorn chick: Rate manipulations. The Journal of the Acoustical Society of America 95 (4), 2136–2144.

Burkard, R., McGee, J., Walsh, E.J., 1996. Effects of stimulus rate on the feline brain-stem auditory evoked response during development. I. Peak latencies. The Journal of the Acoustical Society of America 100 (2), 978–990.

Burkard, R., Voigt, H.F., 1989. Stimulus dependencies of the gerbil brain-stem auditory-evoked response (BAER). I: Effects of click level, rate, and polarity. The Journal of the Acoustical Society of America 85 (6), 2514–2525.

Burkard, R.F., Sims, D., 2001. The human auditory brainstem response to high click rates.

Burton, J.A., Tarabillo, A.L., Finnie, K.R., Shuster, K.A., Mackey, C.A., Hackett, T.A., Ramachandran, R.R., 2022. Chronic otitis secondary to tympanic membrane electrode placement in macaque monkeys (*Macaca mulatta*). Comparative Medicine 72 (2), 104–112.

Burton, J.A., Valero, M.D., Hackett, T.A., Ramachandran, R., 2019. The use of nonhuman primates in studies of noise injury and treatment. Journal of Acoustic Society of America 146 (5), 3770–3789.

Carhart, R., Jerger, J.F., 1959. Preferred method for clinical determination of pure–tone thresholds. Journal of speech and hearing disorders 24 (4), 330–345.

Cashman, M., Rossman, R., 1983. Diagnostic features of the auditory brainstem response in identifying cerebellopontine angle tumours. Scandinavian audiology 12 (1), 35–41.

Chambers, R.D., Matthies, M.L., Griffiths, S.K., 1989. Correlations between various measures of head size and auditory brainstem response latencies. Hearing research 41 (2-3), 179–187.

Chang, K.W., Norton, S.J., 1996. The effects of continuous versus interrupted noise exposures on distortion product otoacoustic emissions in guinea pigs. Hearing research 96 (1-2), 1–12.

Chiou, K.L., Montague, M.J., Goldman, E.A., Watowich, M.M., Sams, S.N., Song, J., Horvath, J.E., Sterner, K.N., Ruiz-Lambides, A.V., Martínez, M.I., 2020. Rhesus macaques as a tractable physiological model of human ageing. Philosophical Transactions of the Royal Society B 375 (1811), 20190612.

Cicchetti, D.V., 1994. Guidelines, criteria, and rules of thumb for evaluating normed and standardized assessment instruments in psychology. Psychological assessment 6 (4), 284.

Conti, G., Modica, V., Castrataro, A., Fileni, A., Colosimo Jr., C., 1988. Latency of the auditory brainstem response (ABR) and head size. Evidence of the relationship by means of radiographic data. Scand Audiol Suppl 30, 219–223.

Crumley, W., 2011. Good practices in auditory brainstem response, part 1. Retrieved November 16, 2013.

Daly, D., Roeser, R., Aung, M., Daly, D., 1977. Early evoked potentials in patients with acoustic neuroma. Electroencephalography and clinical Neurophysiology 43 (2), 151–159.

Davis, H., 1976. Principles of electric response audiometry. Ann Otol Rhinol Laryngol 85 (SUPPL 28), 1–96 3 Pt3.

Davis, R.T., Leathers, C.W., 1985. Behavior and pathology of aging in rhesus monkeys.

Di Mauro, R., Di Girolamo, S., Ralli, M., de Vincentiis, M., Mercuri, N., Albanese, M., 2019. Subclinical cochlear dysfunction in newly diagnosed relapsing-remitting multiple sclerosis. Multiple sclerosis and related disorders 33, 55–60.
Don, M., Allen, A.R., Starr, A., 1977. Effect of click rate on the latency of auditory brain stem responses in humans. Annals of Otology. Rhinology & Laryngology 86 (2), 186–195.
Don, M., Ponton, C.W., Eggermont, J.J., Masuda, A., 1993. Gender differences in cochlear response time: An explanation for gender amplitude differences in the unmasked auditory brain-stem response. The Journal of the Acoustical Society of America 94 (4), 2135–2148.
Don, M., Ponton, C.W., Eggermont, J.J., Masuda, A., 1994. Auditory brainstem response (ABR) peak amplitude variability reflects individual differences in cochlear response times. The Journal of the Acoustical Society of America 96 (6), 3476–3491.
Doyle, W.J., Saad, M.M., Fria, T.J., 1983. Maturation of the auditory brain stem response in rhesus monkeys (Macaca mulatta). Electroencephalogr Clin Neurophysiol 56 (2), 210–223. doi:10.1016/0013-4694(83)90075-5.
Durakovic, N., Valente, M., Goebel, J.A., Wick, C.C., 2019. What defines asymmetric sensorineural hearing loss? The Laryngoscope 129 (5), 1023–1024.
Dylla, M., Hrnicek, A., Rice, C., Ramachandran, R., 2013. Detection of tones and their modification by noise in nonhuman primates. Journal of the Association for Research in Otolaryngology 14 (4), 547–560.
Engle, J.R., Gray, D.T., Turner, H., Udell, J.B., Recanzone, G.H., 2014. Age-related neurochemical changes in the rhesus macaque inferior colliculus. Front Aging Neurosci 6, 73. doi:10.3389/fnagi.2014.00073.
Feldman, A.S., 1977. Diagnostic application and interpretation of tympanometry and the acoustic reflex. Audiology 16 (4), 294–306.
Ferraro, J.A., City, K., 2000. Clinical electrocochleography: overview of theories, techniques and applications. Audiology Online.
Ferraro, J.A., Murphy, G.B., Ruth, R.A., 1986. A comparative study of primary electrodes used in extratympanic electrocochleography. In: Seminars in Hearing. Copyright© 1986 by Thieme Medical Publishers, Inc., pp. 279–286.
Ferraro, J.A., Tibbils, R.P., 1999. SP/AP area ratio in the diagnosis of Meniere's disease. Am J Audiol 8 (1), 21–28. doi:10.1044/1059-0889(1999/001).
Fria, T.J., 1980. The auditory brain stem response: background and clinical applications. Educational Publications Divisions, Maico Hearing Instruments.
Fria, T.J., Saad, M.M., Doyle, W.J., Cantekin, E.I., 1982. Auditory brain stem responses in rhesus monkey with otitis media with effusion. Otolaryngology—Head and Neck Surgery 90 (6), 824–830.
Furman, A.C., Kujawa, S.G., Liberman, M.C., 2013. Noise-induced cochlear neuropathy is selective for fibers with low spontaneous rates. Journal of Neurophysiology 110 (3), 577–586. doi:10.1152/jn.00164.2013.
Galambos, R., Hecox, K., 1977. Clinical applications of the brain stem auditory evoked potentials. Auditory Evoked PotentQls in Man Psychopharmacology Correlates of Evoked Potentials.
Gibbs, R.A., Rogers, J., Katze, M.G., Bumgarner, R., Weinstock, G.M., Mardis, E.R., Remington, K.A., Strausberg, R.L., Venter, J.C., Wilson, R.K., Batzer, M.A., Bustamante, C.D., Eichler, E.E., Hahn, M.W., Hardison, R.C., Makova, K.D., Miller, W., Milosavljevic, A., Palermo, R.E., Siepel, A., Sikela, J.M., Attaway, T., Bell, S., Bernard, K.E., Buhay, C.J., Chandrabose, M.N., Dao, M., Davis, C., Delehaunty, K.D., Ding, Y., Dinh, H.H., Dugan-Rocha, S., Fulton, L.A., Gabisi, R.A., Garner, T.T., Godfrey, J., Hawes, A.C., Hernandez, J., Hines, S., Holder, M., Hume, J., Jhangiani, S.N., Joshi, V., Khan, Z.M., Kirkness, E.F., Cree, A., Fowler, R.G., Lee, S., Lewis, L.R., Li, Z., Liu, Y.S., Moore, S.M., Muzny, D., Nazareth, L.V., Ngo, D.N., Okwuonu, G.O., Pai, G., Parker, D., Paul, H.A., Pfannkoch, C., Pohl, C.S., Rogers, Y.H., Ruiz, S.J., Sabo, A., Santibanez, J., Schneider, B.W., Smith, S.M., Sodergren, E., Svatek, A.F., Utterback, T.R., Vattathil, S., Warren, W., White, C.S., Chinwalla, A.T., Feng, Y., Halpern, A.L., Hillier, L.W., Huang, X., Minx, P., Nelson, J.O., Pepin, K.H., Qin, X., Sutton, G.G., Venter, E., Walenz, B.P., Wallis, J.W., Worley, K.C., Yang, S.P., Jones, S.M., Marra, M.A., Rocchi, M., Schein, J.E., Baertsch, R., Clarke, L., Csuros, M., Glasscock, J., Harris, R.A., Havlak, P., Jackson, A.R., Jiang, H., Liu, Y., Messina, D.N., Shen, Y., Song, H.X., Wylie, T., Zhang, L., Birney, E., Han, K., Konkel, M.K., Lee, J., Smit, A.F., Ullmer, B., Wang, H., Xing, J., Burhans, R., Cheng, Z., Karro, J.E., Ma, J., Raney, B., She, X., Cox, M.J., Demuth, J.P., Dumas, L.J., Han, S.G., Hopkins, J., Karimpour-Fard, A., Kim, Y.H., Pollack, J.R., Vinar, T., Addo-Quaye, C., Degenhardt, J., Denby, A., Hubisz, M.J., Indap, A., Kosiol, C., Lahn, B.T., Lawson, H.A., Marklein, A., Nielsen, R., Vallender, E.J., Clark, A.G., Ferguson, B., Hernandez, R.D., Hirani, K., Kehrer-Sawatzki, H., Kolb, J., Patil, S., Pu, L.L., Ren, Y., Smith, D.G., Wheeler, D.A., Schenck, I., Ball, E.V., Chen, R., Cooper, D.N., Giardine, B., Hsu, F., Kent, W.J., Lesk, A., Nelson, D.L., O'Brien, W.E., Prufer, K., Stenson, P.D., Wallace, J.C., Ke, H., Liu, X.M., Wang, P., Xiang, A.P., Yang, F., Barber, G.P., Haussler, D., Karolchik, D., Kern, A.D., Kuhn, R.M., Smith, K.E., Zwieg, A.S., 2007. Evolutionary and biomedical insights from the rhesus macaque genome. Science 316 (5822), 222–234. doi:10.1126/science.1139247.
Gorga, M.P., Kaminski, J.R., Beauchaine, K.A., Jesteadt, W., 1988. Auditory brainstem responses to tone bursts in normally hearing subjects. J Speech Hear Res 31 (1), 87–97. doi:10.1044/jshr.3101.87.
Gorga, M.P., Neely, S.T., Bergman, B., Beauchaine, K.L., Kaminski, J.R., Peters, J., Jesteadt, W., 1993. Otoacoustic emissions from normal-hearing and hearing-impaired subjects: distortion product responses. Journal of the Acoustical Society of America 93 (4), 2050–2060. doi:10.1121/1.406691.
Gorga, M.P., Reiland, J.K., Beauchaine, K.A., Worthington, D.W., Jesteadt, W., 1987. Auditory brainstem responses from graduates of an intensive care nursery: normal patterns of response. Journal of Speech, Language, and Hearing Research 30 (3), 311–318.
Grose, J.H., Buss, E., Hall Iii, J.W., 2017. Loud music exposure and cochlear synaptopathy in young adults: Isolated auditory brainstem response effects but no perceptual consequences. Trends in hearing 21, 2331216517737417.
Hall, J., 2017. Rethinking your diagnostic audiology battery: Using value added tests. Audiology Online.
Hecox, K., Galambos, R., 1974. Brain stem auditory evoked responses in human infants and adults. Archives of otolaryngology 99 (1), 30–33.
Henry, K.S., Gall, M.D., Bidelman, G.M., Lucas, J.R., 2011. Songbirds tradeoff auditory frequency resolution and temporal resolution. Journal of Comparative Physiology A 197 (4), 351–359.
Hind, S.E., Haines-Bazrafshan, R., Benton, C.L., Brassington, W., Towle, B., Moore, D.R., 2011. Prevalence of clinical referrals having hearing thresholds within normal limits. International journal of audiology 50 (10), 708–716.
Huang, Q., Qiu, Z., Zhang, Z., Ou, Y., Yang, H., Zheng, Y., 2011. [Utility of Sp/Ap curve area ratio electrocochleography in diagnosis of Meniere's disease]. Lin Chung Er Bi Yan Hou Tou Jing Wai Ke Za Zhi 25 (1), 8–10.
Hurley, R.M., Sells, J.P., 2003. An abbreviated word recognition protocol based on item difficulty. Ear and hearing 24 (2), 111–118.
Hyde, M., Blair, R., 1981. The auditory brainstem response in neuro-otology: perspectives and problems. The Journal of otolaryngology 10 (2), 117–125.
Jerger, J., Anthony, L., Jerger, S., Mauldin, L., 1974. Studies in impedance audiometry: III. Middle ear disorders. Archives of Otolaryngology 99 (3), 165–171.
Kemp, D.T., 2002. Otoacoustic emissions, their origin in cochlear function, and use. British medical bulletin 63 (1), 223–241.
Kohrman, D.C., Wan, G., Cassinotti, L., Corfas, G., 2020. Hidden hearing loss: A disorder with multiple etiologies and mechanisms. Cold Spring Harbor perspectives in medicine 10 (1), a035493.
Kraus, N., Smith, D.I., Reed, N.L., Willott, J., Erwin, J., 1985. Auditory brainstem and middle latency responses in non-human primates. Hear Res 17 (3), 219–226. doi:10.1016/0378-5955(85)90066-8.
Krieg, S.M., Kempf, L., Droese, D., Rosahl, S.K., Meyer, B., Lehmberg, J., 2014. Superiority of tympanic ball electrodes over mastoid needle electrodes for intraoperative monitoring of hearing function. Journal of Neurosurgery 120 (5), 1042–1047.
Kujawa, S.G., Liberman, M.C., 2009. Adding insult to injury: cochlear nerve degeneration after "temporary" noise-induced hearing loss. Journal of Neuroscience 29 (45), 14077–14085. doi:10.1523/JNEUROSCI.2845-09.2009.
Kummer, P., Janssen, T., Arnold, W., 1998. The level and growth behavior of the 2 f1− f2 distortion product otoacoustic emission and its relationship to auditory sensitivity in normal hearing and cochlear hearing loss. The Journal of the Acoustical Society of America 103 (6), 3431–3444.
Lasky, R.E., Maier, M.M., Snodgrass, E.B., Laughlin, N.K., Hecox, K.E., 1995a. Auditory evoked brainstem and middle latency responses in Macaca mulatta and humans. Hearing research 89 (1-2), 212–225.
Lasky, R.E., Snodgrass, E.B., Laughlin, N.K., Hecox, K.E., 1995b. Distortion product otoacoustic emissions in Macaca mulatta and humans. Hearing research 89 (1-2), 35–51.
Lasky, R.E., Soto, A.A., Luck, M.L., Laughlin, N.K., 1999. Otoacoustic emission, evoked potential, and behavioral auditory thresholds in the rhesus monkey (Macaca mulatta). Hearing research 136 (1-2), 35–43.
Lauter, J.L., Loomis, R.L., 1988. Individual differences in auditory electric responses: comparisons of between-subject and within-subject variability II. Amplitude of brainstem vertex-positive peaks. Scandinavian Audiology 17 (2), 87–92.
Lee, J.-H., Lee, M.Y., Choi, J.E., Jung, J.Y., 2020. Auditory Brainstem Response to Paired Click Stimulation as an Indicator of Peripheral Synaptic Health in Noise-Induced Cochlear Synaptopathy. Frontiers in Neuroscience 14.
Lee, J.-H., Lee, M.Y., Choi, J.E., Jung, J.Y., 2021. Auditory brainstem response to paired click stimulation as an indicator of peripheral synaptic health in noise-induced cochlear synaptopathy. Frontiers in Neuroscience 1377.
Liberman, M., Zuo, J., Guinan Jr., J., 2004. Otoacoustic emissions without somatic motility: can stereocilia mechanics drive the mammalian cochlea? The Journal of the Acoustical Society of America 116 (3), 1649–1655.
Lidén, G., Peterson, J.L., Björkman, G., 1970. Tympanometry. Archives of Otolaryngology 92 (3), 248–257.
Lin, H.W., Furman, A.C., Kujawa, S.G., Liberman, M.C., 2011. Primary neural degeneration in the Guinea pig cochlea after reversible noise-induced threshold shift. Journal of the Association for Research in Otolaryngology 12 (5), 605–616. doi:10.1007/s10162-011-0277-0.
Lobarinas, E., Salvi, R., Ding, D., 2016. Selective inner hair cell dysfunction in chinchillas impairs hearing-in-noise in the absence of outer hair cell loss. Journal of the Association for Research in Otolaryngology 17 (2), 89–101.
Lonsbury-Martin, B.L., Martin, G.K., 1990. The clinical utility of distortion-product otoacoustic emissions. Ear and Hearing 11 (2), 144–154. doi:10.1097/00003446-199004000-00009.
Mackey, C., Tarabillo, A., Ramachandran, R., 2021. Three psychophysical metrics of auditory temporal integration in macaques. The Journal of the Acoustical Society of America 150 (4), 3176–3191.
Marco, J., Morant, A., Caballero, J., Ortells, I., Paredes, C., Brines, J., 1995. Distortion product otoacoustic emissions in healthy newborns: normative data. Acta oto-laryngologica 115 (2), 187–189.
Martin, G.K., Vazquez, A.E., Jimenez, A.M., Stagner, B.B., Howard, M.A., Lonsbury–Martin, B.L., 2007. Comparison of distortion product otoacoustic emissions in 28 inbred strains of mice. Hearing research 234 (1-2), 59–72.
Matlab, V., 2010. 7.10. 0 (R2010a). The MathWorks Inc., Natick, Massachusetts.

Mitchell, C., Phillips, D.S., Trune, D.R., 1989. Variables affecting the auditory brainstem response: audiogram, age, gender and head size. Hearing Research 40 (1-2), 75–85. doi:10.1016/0378-5955(89)90101-9.
Musiek, F.E., Kibbe, K., Rackliffe, L., Weider, D.J., 1984. The auditory brain stem response I-V amplitude ratio in normal, cochlear, and retrocochlear ears. Ear and hearing 5 (1), 52–55.
Newton, E.H., Cooper Jr., W.A., Coleman, J.R., 1992. Rate and frequency interactions in the auditory brainstem response of the adult rat. Hear Res 60 (1), 73–79. doi:10.1016/0378-5955(92)90060-z.
Ng, C.W., Navarro, X., Engle, J.R., Recanzone, G.H., 2015. Age-related changes of auditory brainstem responses in nonhuman primates. J Neurophysiol 114 (1), 455–467. doi:10.1152/jn.00663.2014.
Ng, I.H.-Y., Mcpherson, B., 2005. Test-retest reliability of distortion product otoacoustic emissions in the 1 to 7 kHz range. Audiological Medicine 3 (2), 108–115.
Norton, S.J., Gorga, M.P., Widen, J.E., Folsom, R.C., Sininger, Y., Cone-Wesson, B., Vohr, B.R., Mascher, K., Fletcher, K., 2000. Identification of neonatal hearing impairment: evaluation of transient evoked otoacoustic emission, distortion product otoacoustic emission, and auditory brain stem response test performance. Ear Hear 21 (5), 508–528. doi:10.1097/00003446-200010000-00013.
Ohashi, T., Ochi, K., Nishino, H., Kenmochi, M., Yoshida, K., 2005. Recovery of human compound action potential using a paired-click stimulation paradigm. Hearing research 203 (1-2), 192–200.
Parham, K., 1997. Distortion product otoacoustic emissions in the C57BL/6J mouse model of age-related hearing loss. Hearing research 112 (1-2), 216–234.
Parham, K., Zhao, H.-B., Ye, Y., Kim, D., 1998. Responses of anteroventral cochlear nucleus neurons of the unanesthetized decerebrate cat to click pairs as simulated echoes. Hearing research 125 (1-2), 131–146.
Park, J.Y., Clark, W.W., Coticchia, J.M., Esselman, G.H., Fredrickson, J.M., 1995. Distortion product otoacoustic emissions in rhesus (Macaca mulatta) monkey ears: normative findings. Hearing research 86 (1-2), 147–162.
Passingham, R., 2009. How good is the macaque monkey model of the human brain? Current opinion in neurobiology 19 (1), 6–11.
Petersen, L., Wilson, W.J., Kathard, H., 2018. Towards the preferred stimulus parameters for distortion product otoacoustic emissions in adults: A preliminary study. South African Journal of Communication Disorders 65 (1), 1–10.
Pfingst, B.E., Laycock, J., Flammino, F., Lonsbury-Martin, B., Martin, G., 1978. Pure tone thresholds for the rhesus monkey. Hearing Research 1 (1), 43–47. doi:10.1016/0378-5955(78)90008-4.
Picton, T.W., Woods, D.L., Baribeau-Braun, J., Healey, T.M., 1977. Evoked potential audiometry. J Otolaryngol 6 (2), 90–119.
Pienkowski, M., Ulfendahl, M., 2011. Differential Effects of Salicylate, Quinine, and Furosemide on Guinea Pig Inner and Outer Hair Cell Function Revealed by the Input–Output Relation of the Auditory Brainstem Response. Journal of the American Academy of Audiology 22 (02), 104–112.
Prendergast, G., Tu, W., Guest, H., Millman, R.E., Kluk, K., Couth, S., Munro, K.J., Plack, C.J., 2018. Supra-threshold auditory brainstem response amplitudes in humans: Test-retest reliability, electrode montage and noise exposure. Hear Res 364, 38–47. doi:10.1016/j.heares.2018.04.002.
Qin, Z., Wood, M., Rosowski, J.J., 2010. Measurement of conductive hearing loss in mice. Hearing research 263 (1-2), 93–103.
Rance, G., Beer, D.E., Cone-Wesson, B., Shepherd, R.K., Dowell, R.C., King, A.M., Rickards, F.W., Clark, G.M., 1999. Clinical findings for a group of infants and young children with auditory neuropathy. Ear Hear 20 (3), 238–252. doi:10.1097/00003446-199906000-00006.
Rilling, J.K., Insel, T.R., 1999. The primate neocortex in comparative perspective using magnetic resonance imaging. Journal of human evolution 37 (2), 191–223.
Roth, G.S., Mattison, J.A., Ottinger, M.A., Chachich, M.E., Lane, M.A., Ingram, D.K., 2004. Aging in rhesus monkeys: relevance to human health interventions. Science 305 (5689), 1423–1426.
Rowe III, M.J., 1978. Normal variability of the brain-stem auditory evoked response in young and old adult subjects. Electroencephalography and Clinical Neurophysiology 44 (4), 459–470.
Schwartz, D.M., Berry, G., 1985. Normative aspects of the ABR. The auditory brainstem response 65–97.
Sergeyenko, Y., Lall, K., Liberman, M.C., Kujawa, S.G., 2013. Age-related cochlear synaptopathy: an early-onset contributor to auditory functional decline. J Neurosci 33 (34), 13686–13694. doi:10.1523/JNEUROSCI.1783-13.2013.
Shaffer, L., Long, G., 2004. Low-frequency distortion product otoacoustic emissions in two species of kangaroo rats: implications for auditory sensitivity. Journal of Comparative Physiology A 190 (1), 55–60.
Shi, L., Chang, Y., Li, X., Aiken, S.J., Liu, L., Wang, J., 2016. Coding deficits in noise-induced hidden hearing loss may stem from incomplete repair of ribbon synapses in the cochlea. Frontiers in neuroscience 10, 231.
Shrout, P.E., Fleiss, J.L., 1979. Intraclass correlations: uses in assessing rater reliability. Psychological bulletin 86 (2), 420.
Sininger, Y.S., 1993. Auditory brain stem response for objective measures of hearing. Ear and hearing 14 (1), 23–30.
Sininger, Y.S., Abdala, C., Cone-Wesson, B., 1997. Auditory threshold sensitivity of the human neonate as measured by the auditory brainstem response. Hearing research 104 (1-2), 27–38.
Skoe, E., Tufts, J., 2018. Evidence of noise-induced subclinical hearing loss using auditory brainstem responses and objective measures of noise exposure in humans. Hearing research 361, 80–91.
Smith, S., Krizman, J., Liu, C., White-Schwoch, T., Nicol, T., Kraus, N., 2019. Investigating peripheral sources of speech-in-noise variability in listeners with normal audiograms. Hearing research 371, 66–74.
Sohmer, H., Feinmesser, M., 1967. Cochlear action potentials recorded from the external ear in man. Ann Otol Rhinol Laryngol 76 (2), 427–435. doi:10.1177/000348946707600211.
Song, Q., Shen, P., Li, X., Shi, L., Liu, L., Wang, J., Yu, Z., Stephen, K., Aiken, S., Yin, S., Wang, J., 2016. Coding deficits in hidden hearing loss induced by noise: the nature and impacts. Scientific Reports 6, 25200. doi:10.1038/srep25200.
Spankovich, C., Le Prell, C.G., Lobarinas, E., Hood, L.J., 2017. Noise history and auditory function in young adults with and without type 1 diabetes mellitus. Ear and hearing 38 (6), 724–735.
Stach, B.A., Ramachandran, V., 2021. Clinical audiology: An introduction. Plural Publishing.
Stapells, D.R., Oates, P., 1997. Estimation of the pure-tone audiogram by the auditory brainstem response: a review. Audiology and Neurootology 2 (5), 257–280. doi:10.1159/000259252.
Starr, A., 1976. Correlation between confirmed sites of neurological lesions and abnormalities of far-field auditory brainstem responses. Electroencephalography and clinical neurophysiology 41 (6), 595–608.
Starr, A., Picton, T.W., Sininger, Y., Hood, L.J., Berlin, C.I., 1996. Auditory neuropathy. Brain 119 (3), 741–753.
Starr, A., Sininger, Y., Nguyen, T., Michalewski, H.J., Oba, S., Abdala, C., 2001. Cochlear receptor (microphonic and summating potentials, otoacoustic emissions) and auditory pathway (auditory brain stem potentials) activity in auditory neuropathy. Ear Hear 22 (2), 91–99. doi:10.1097/00003446-200104000-00002.
Stockard, J., Stockard, J., Sharbrough, F., 1977. Detection and localization of occult lesions with brainstem auditory responses. Mayo Clinic Proceedings, pp. 761–769.
Stockard, J.J., Stockard, J.E., Sharbrough, F.W., 1978. Nonpathologic factors influencing brainstem auditory evoked potentials. American Journal of EEG technology 18 (4), 177–209.
Supin, A.Y., Popov, V.V., 1995. Temporal resolution in the dolphin's auditory system revealed by double-click evoked potential study. The Journal of the Acoustical Society of America 97 (4), 2586–2593.
Tanaka, H., Komatsuzaki, A., Hentona, H., 1996. Usefulness of auditory brainstem responses at high stimulus rates in the diagnosis of acoustic neuroma. ORL 58 (4), 224–228.
Thornton, A.R., Raffin, M.J., 1978. Speech-discrimination scores modeled as a binomial variable. Journal of speech and hearing research 21 (3), 507–518.
Torre 3rd, P., Fowler, C.G., 2000. Age-related changes in auditory function of rhesus monkeys (Macaca mulatta). Hear Res 142 (1-2), 131–140. doi:10.1016/s0378-5955(00)00025-3.
Torre, P., Lasky, R.E., Fowler, C.G., 2000. Aging and Middle Ear Function in Rhesus Monkeys (Macaca mulatta): Envejecimiento y funcion del oido medio en monos Rhesus [Macaca mulatta. Audiology 39 (6), 300–304.
Trune, D.R., Mitchell, C., Phillips, D.S., 1988. The relative importance of head size, gender and age on the auditory brainstem response. Hearing Research 32 (2-3), 165–174. doi:10.1016/0378-5955(88)90088-3.
Valero, M.D., Burton, J.A., Hauser, S.N., Hackett, T.A., Ramachandran, R., Liberman, M.C., 2017. Noise-induced cochlear synaptopathy in rhesus monkeys (Macaca mulatta). Hearing Research 353, 213–223. doi:10.1016/j.heares.2017.07.003.
Valero, M.D., Ratnam, R., 2011. Reliability of distortion-product otoacoustic emissions in the common marmoset (Callithrix jacchus). Hearing research 282 (1-2), 265–271.
Wada, H., Ohyama, K., Kobayashi, T., Koike, T., Noguchi, S.-I., 1995. Effect of middle ear on otoacoustic emissions. Audiology 34 (4), 161–176.
Walsh, E.J., McGee, J., Javel, E., 1986. Development of auditory-evoked potentials in the cat. III. Wave amplitudes. J Acoust Soc Am 79 (3), 745–754. doi:10.1121/1.393463.
Walton, J., Orlando, M., Burkard, R., 1999. Auditory brainstem response forward–masking recovery functions in older humans with normal hearing. Hearing research 127 (1-2), 86–94.
Wever, E.G., 1949. Theory of hearing.
Wilson, R.H., Noe, C.M., Cruickshanks, K.J., Wiley, T.L., Nondahl, D.M., 2010. Prevalence and degree of hearing loss among males in the Beaver Dam Cohort: A comparison of veterans and non-veterans. Journal of rehabilitation research and development 47 (6), 505.
Wysocki, L.E., Ladich, F., 2002. Can fishes resolve temporal characteristics of sounds? New insights using auditory brainstem responses. Hearing research 169 (1-2), 36–46.
Zar, J.H., 2005. Spearman rank correlation. Encyclopedia of biostatistics 7.
Zehnder, A.F., Kristiansen, A.G., Adams, J.C., Kujawa, S.G., Merchant, S.N., McKenna, M.J., 2006. Osteoprotegrin knockout mice demonstrate abnormal remodeling of the otic capsule and progressive hearing loss. The Laryngoscope 116 (2), 201–206.
Zhou, X., Jen, P.H., Seburn, K.L., Frankel, W.N., Zheng, Q.Y., 2006. Auditory brainstem responses in 10 inbred strains of mice. Brain Res 1091 (1), 16–26. doi:10.1016/j.brainres.2006.01.107.